The construction of an ellipsometer to measure the refractive index and thickness of thin films.

DICK, D.A.

1975

THE CONSTRUCTION OF AN ELLIPSOMETER TO MEASURE THE REFRACTIVE INDEX AND THICKNESS OF THIN FILMS

by

David Allan Dick, BSc

A Thesis presented in application for the Degree of Master of Philosophy of the Council for National Academic Awards. The research was conducted in the School of Physics, Robert Gordon's Institute of Technology, Aberdeen.

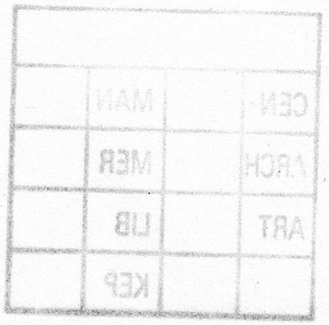

SEPTEMBER, 1975

ACKNOWLEDGEMENTS

The work described in this thesis was carried out in the School of Physics, Robert Gordon's Institute of Technology, and thanks are due to the Governors for providing the facilities for the research, and for their financial support.

The author would like to express his appreciation to Dr W R Oliver, for his expert help and advice in his capacity as supervisor, and for his personal interest during the preparation of the thesis; to Dr W J Bates of the Department of Natural Philosophy, University of Aberdeen, and Dr R J King, Department of Metrology, National Physical Laboratory, for their valuable suggestions and discussion; and to Dr W M Lister, of the School of Mathematics, for his assistance with mathematical difficulties.

The generous assistance afforded by Mr J Ward of OCLI, Optical Coatings Ltd., particularly with the deposition of the MgF_2 films described in this thesis, is gratefully acknowledged.

Thanks are also due to Mr A Middleton of the School of Physics for his able technical assistance and to Mr W Black for his photographic expertise.

The author is indebted to the staff of the School of Physics, and others who directly or indirectly helped in this work, particularly Miss P Swanson for typing this thesis.

ABSTRACT

The ellipsometer, like all precision optical instruments, is a delicate piece of equipment requiring care in its construction, maintenance and operation. Since multiple reflections and birefringence in the optical components introduce large instrumental errors, a correct choice of component parts must be made so as to minimise these effects.

This thesis is an account of the construction of an ellipsometer for use in measuring the thickness and refractive index of thin dielectric films. An attempt has been made to rationalise the mathematical approach and to present a valid method for the evaluation of results.

The first Chapter is a general introduction to methods for measuring the thickness and/or refractive index of thin films and surfaces. Chapter 2 develops the fundamental equation of ellipsometry from the problem of reflection and refraction of light at a boundary between two homogeneous, isotropic media, and reflection from a film-covered surface. The construction and choice of components for the ellipsometer is outlined in Chapter 3 while in Chapter 4 the alignment of the instrument and the various components, is discussed.

Chapter 5 introduces the relationship between the parameters of ellipsometry and presents various data handling methods as well as the computer program used in this thesis. An evaluation of the instrument is given in Chapter 6 with actual results taken using the instrument and the order of accuracy found.

TABLE OF CONTENTS

-----oooOooo-----

CHAPTER 1

INTRODUCTION

Recent advances in high-vacuum techniques have resulted in increased interest, initially on evaporated thin films used mainly for numerous optical purposes, but latterly in metallic, insulating and semiconducting thin films which are used in both active and passive electronic devices.

The method employed in the determination of the properties of thin films depends on several factors, such as the accessibility of an edge allowing interference methods to be used, whether or not the films and/or substrates are transparent, and whether measurement might have to be made in situ. Techniques of the latter type usually allow for monitoring and controlling of the deposition rate as well as thickness measurement. There are five main methods for determining film thickness: electrical, mechanical, microbalance, radiation - absorption/emission, and optical. It may be noted that any physical quantity related to film thickness can, in principle, be used to measure film thickness.

In the optical determination of surfaces and films on substrates the three basic measurements are photometric, interferometric and polarimetric. These methods are well reviewed by Heavens (1965), Mayer (1950), Behrndt (1966), Rouard and Bousquet (1965), and Abelès (1963). The relative advantages of these optical methods depend on factors which include the purpose of measurement, sample size and preparation restrictions, as well as the accuracy and sensitivity required.

1.1.0 Photometric Methods

When a transparent substrate has a transparent or slightly absorbing film of differing refractive index deposited upon it, the transmittance and optical reflectance of the combination shows an oscillatory pattern with increasing film thickness due to interference effects. Schopper (1952) describes a /

a method which entails the measurement of the amplitude and phase of the light reflected from each side of the film and of the light transmitted by the film, all measurements being as near as possible to normal incidence. Another method is that of Malé (1952) in which the thickness and optical constants are determined from reflectances and transmittances. Other methods are those of David (1937), Murmann (1933) and Wolter (1937).

1.1.1 Spectrophotometric Methods

When white light is incident upon a thin film covering a substrate of different refractive index, the reflected light will show a maximum for various wavelengths for which the interference condition is satisfied producing a characteristic hue of the film. Judgement of the colour is subjective and breaks down for thick films. Jacquinot (1942) shows how a spectrophotometer may be employed to measure the transmitted or reflected intensity as a function of the wavelength, while Dumin (1967) uses a double beam recording spectrophotometer to measure the thickness of epitaxial semiconductor films deposited on a substrate of different refractive index. A very simple method due to Abelès (1949) can be used to determine the refractive index alone. It makes use of Brewster's Law and the fact that at the polarizing angle of incidence (see the end of section 2.1.3)for the air-film interface, the reflection factor of the film plus the substrate is equal to that of the bare substrate.

1.2.0 Interferometric Methods

The measurement of interference fringes produced when two reflecting surfaces are brought into close proximity enables a direct and accurate determination of the film thickness and surface topography to be made. There are three methods. Pliskin and Conrad (1964) describe a variable-angle /

variable-angle monochromatic fringe observation (VAMFO) arrangement to measure the refractive index and thickness of transparent films on reflecting substrates. Of the other two methods, one employs Fizeau fringes of constant thickness while the other uses fringes of equal chromatic order. The interference-fringe methods, developed mainly by Tolansky (1960) are now accepted as the absolute-standard methods of thin film measurement. The use of the Fabry-Perot and Michelson interferometers for film thickness measurement have been described by Schultz (1950) and Fochs (1950).

1.3.0 Polarimetric Methods

These are perhaps the oldest methods for the study of thin films dating back to the 1880's and make use of the fact that measurements of the state of polarization of a light beam may be made with high accuracy. The principle is as follows: a beam of plane polarized light, usually polarized at an angle of 45° to the plane of incidence, is reflected by the thin film at oblique incidence and the properties of the reflected elliptically polarized light are analysed. The term ellipsometry, originally introduced by Rothen (1945), may be used to describe techniques in which only the shape, azimuth and handedness of the ellipse are found.

This thesis develops a low cost ellipsometer of typical configuration through to its conclusion as a sensitive instrument for measuring the refractive index and thickness of thin films. The starting point for the study of thin films is the predictions of electro-magnetic theory. It is worth noting that when the films are made from layers of thickness of molecular dimensions, the investigation is essentially a scattering problem (Heavens, 1960).

CHAPTER 2

CLASSICAL THEORY OF FILM OPTICS

2.1.0 Reflection and Refraction of Light at a Boundary between Two Dielectric Media

2.1.1 Maxwell's Equations

Maxwell's chief concern in the generalisation of the two well established concepts, Ampère's circuital law and Neumann's equation, was that in differential form they led to the following famous equations (for a right-handed set of Cartesian axes) the proofs of which are given by Fewkes and Yarwood (1965):

$$\frac{\partial H_z}{\partial y} - \frac{\partial H_y}{\partial z} = j_x + \frac{\partial D_x}{\partial t} \qquad \text{---- (2.1.1a)}$$

$$\frac{\partial H_x}{\partial z} - \frac{\partial H_z}{\partial x} = j_y + \frac{\partial D_y}{\partial t} \qquad \text{---- (2.1.1b)}$$

$$\frac{\partial H_y}{\partial x} - \frac{\partial H_x}{\partial y} = j_z + \frac{\partial D_z}{\partial t} \qquad \text{---- (2.1.1c)}$$

where $\vec{H}$ is the magnetic field strength, $\vec{j}$ is the conduction current density, $\vec{D}$ is the electric displacement and x, y and z denote components along x, y and z directions respectively.

$$\frac{\partial E_z}{\partial y} - \frac{\partial E_y}{\partial z} = - \frac{\partial B_x}{\partial t} \qquad \text{---- (2.1.2a)}$$

$$\frac{\partial E_x}{\partial z} - \frac{\partial E_z}{\partial x} = - \frac{\partial B_y}{\partial t} \qquad \text{---- (2.1.2b)}$$

$$\frac{\partial E_y}{\partial x} - \frac{\partial E_x}{\partial y} = - \frac{\partial B_z}{\partial t} \qquad \text{---- (2.1.2c)}$$

where $\vec{E}$ is electric field strength and $\vec{B}$ is the magnetic flux density.

Supplementary /

Supplementary to the above equations are the so-called material equations which describe the properties of matter under the field influence. For isotropic substances these equations are:

$$\vec{j} = \sigma\vec{E} \qquad \text{---- (2.1.3)}$$

$$\vec{D} = \varepsilon\vec{E} \qquad \text{---- (2.1.4)}$$

$$\vec{B} = \mu\vec{H} \qquad \text{---- (2.1.5)}$$

where σ is the conductivity, ε the electric permittivity and μ the magnetic permeability.

Equations (2.1.1) and (2.1.2) in vector calculus form become:

$$\text{curl } \vec{H} = \vec{j} + \frac{\partial \vec{D}}{\partial t} \qquad \text{---- (2.1.6)}$$

$$\text{curl } \vec{E} = -\frac{\partial \vec{B}}{\partial t} \qquad \text{---- (2.1.7)}$$

which in turn for a dielectric become:

$$\text{curl } \vec{H} = \varepsilon \frac{\partial \vec{E}}{\partial t} \qquad \text{---- (2.1.8)}$$

and

$$\text{curl } \vec{E} = -\mu \frac{\partial \vec{H}}{\partial t} \qquad \text{---- (2.1.9)}$$

Finally we have the conditions arising from Gauss's theorem in magnetism and electrostatics:

$$\text{div. } \vec{B} = 0 \qquad \text{---- (2.1.10)}$$

and

$$\text{div. } \vec{D} = \rho \qquad \text{---- (2.1.11)}$$

where ρ is the charge per unit volume in the region.

2.1.2 /

2.1.2 Snell's Laws

Tenquist et al. (1970) show that Maxwell's equations together with the boundary conditions are all that are necessary for the derivation of the laws of refraction and reflection of a plane wave incident at a plane boundary between two homogeneous isotropic media. Figure 2.1 shows the notations for the co-ordinate system. The plane XOY separates the two media, which are characterised by ε_0, μ_0 and ε_1, μ_1. The plane of incidence is XOZ and the angle of incidence is $\emptyset_0$. The amplitudes of the electric vectors of the wave approaching the surface are denoted by E^+_{0p} and E^+_{0s} for the two components, where p refers to the component vector parallel to the plane of incidence and s refers to the component vector normal to the plane of incidence. The reflected wave is denoted by E^-_{0p} and E^-_{0s}. The plus sign is for waves travelling in the forward direction and the minus sign is for waves travelling in the opposite direction. The transmitted wave components are E^+_{1p} and E^+_{1s}.

Coulson (1958) indicates that the space and time dependence of the magnetic and electric vectors of the incident wave can be expressed as proportional to

$$\exp\{i\omega(ct - (\varepsilon_0\mu_0)^{-\frac{1}{2}}(x \sin\emptyset_0 + z \cos\emptyset_0))\}.$$

Similarly the reflected and transmitted waves contain the factors

$$\exp\{i\omega(ct - (\varepsilon_0\mu_0)^{-\frac{1}{2}}(\ell_r x + m_r y + n_r z))\}$$

and

$$\exp\{i\omega(ct - (\varepsilon_1\mu_1)^{-\frac{1}{2}}(\ell_t x + m_t y + n_t z))\},$$

where the subscripts r and t indicate the reflected and transmitted directions respectively, c is the velocity of light, and ω is the angular frequency which is the same for all three waves. For the boundary condition /

condition of continuity of tangential components to be satisfied, the indices of the incident, reflected and transmitted waves must be equal. That is,

$$x \sin\phi_0 + z \cos\phi_0 = \ell_r x + m_r y + n_r z = \ell_t x + m_t y + n_t z$$

Hence it is seen that

(1) The directions of incidence, refraction and reflection are all in the same plane which is normal to the boundary and therefore contains the normal from the coefficients of z. That is, $m_r = m_t = 0$.

(2) Equating coefficients of x the angle of incidence is shown to be equal to the angle of reflection.

(3) Furthermore, the ratio between the sine of the angle of incidence and the sine of the angle of refraction is constant.

That is,

$$\frac{\sin\phi_0}{\sin\phi_1} = \text{constant} = \left(\frac{\mu_1\varepsilon_1}{\mu_0\varepsilon_0}\right)^{\frac{1}{2}}$$

which when $\mu_1 = \mu_0 = 1$ reduces to

$$\frac{\sin\phi_0}{\sin\phi_1} = \left(\frac{\varepsilon_1}{\varepsilon_0}\right)^{\frac{1}{2}} = \frac{n_1}{n_0} \qquad \text{---- (2.1.12)}$$

2.1.3 /

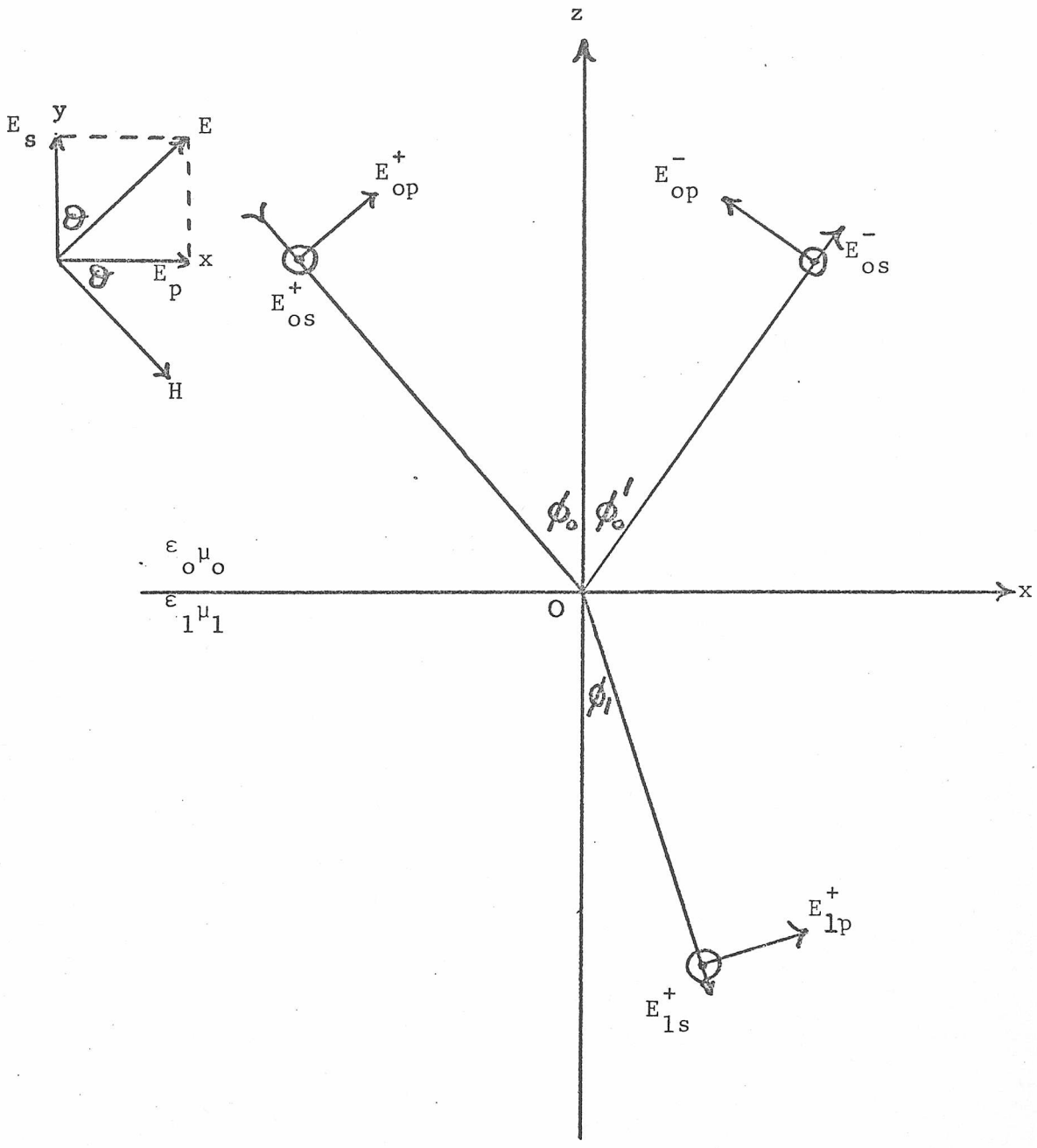

Figure 2.1. Coordinate system showing notations used for the study of the reflection and refraction of a plane wave.

2.1.3 Fresnel's Formulae

The following are the components of the electric and magnetic vectors of the incident wave (i):

$$E^{+}_{Op} = A^{+}_{Op}\cos\phi_O, \quad E^{+}_{Os} = A^{+}_{Os}$$

$$H^{+}_{Op} = -(\varepsilon_O/\mu_O)^{\frac{1}{2}}A^{+}_{Os}\cos\phi_O, \quad H^{+}_{Os} = (\varepsilon_O/\mu_O)^{\frac{1}{2}}A^{+}_{Op}$$

reflected wave (r):

$$E^{-}_{Op} = A^{-}_{Op}\cos\phi_O', \quad E^{-}_{Os} = A^{-}_{Os}$$

$$H^{-}_{Op} = -(\varepsilon_O/\mu_O)^{\frac{1}{2}}A^{-}_{Os}\cos\phi_O', \quad H^{-}_{Os} = (\varepsilon_O/\mu_O)^{\frac{1}{2}}A^{-}_{Op}$$

transmitted wave (t):

$$E^{+}_{1p} = A^{+}_{1p}\cos\phi_1, \quad E^{+}_{1s} = A^{+}_{1s}$$

$$H^{+}_{1p} = -(\varepsilon_1/\mu_1)^{\frac{1}{2}}A^{+}_{1s}\cos\phi_1, \quad H^{+}_{1s} = (\varepsilon_1/\mu_1)^{\frac{1}{2}}A^{+}_{1p}$$

At the boundary between the two dielectric media ($Z = 0$), the tangential components of the field strength vary continuously, ie,

$$E^{+}_{Op} + E^{-}_{Op} = E^{+}_{1p}, \quad E^{+}_{Os} + E^{-}_{Os} = E^{+}_{1s}, \quad H^{+}_{Op} + H^{-}_{Op} = H^{+}_{1p}$$

and

$$H^{+}_{Os} + H^{-}_{Os} = H^{+}_{1s}$$

and since $\cos\phi_O' = -\cos\phi_O$ (the law of reflection) the relation between the amplitude components have the form

$$(A^{+}_{Op} - A^{-}_{Op})\cos\phi_O = A^{+}_{1p}\cos\phi_1 \qquad \text{---- (2.1.13a)}$$

$$A^{+}_{Os} + A^{-}_{Os} = A^{+}_{1s} \qquad \text{---- (2.1.13b)}$$

$(A^{+}_{Os}$ /

$$(A^{+}_{Os} - A^{-}_{Os})Y_O\cos\phi_O = A^{+}_{1s}\, Y_1\cos\phi_1 \qquad \text{---- (2.1.13c)}$$

$$(A^{+}_{Op} + A^{-}_{Op})Y_O = A^{+}_{1p}\, Y_1 \qquad \text{---- (2.1.13d)}$$

where the admittance (Y) of the two media are $Y_O = (\varepsilon_O/\mu_O)^{\frac{1}{2}}$ and $Y_1 = (\varepsilon_1/\mu_1)^{\frac{1}{2}}$ reducing when $\mu_O = \mu_1 = 1$ to the respective refractive indices since $n = (\varepsilon)^{\frac{1}{2}}$.

From equations (2.1.13b) and (2.1.13c),

$$(A^{+}_{Os} - A^{-}_{Os})Y_O\cos\phi_O = (A^{+}_{Os} + A^{-}_{Os})Y_1\cos\phi_1$$

$$\therefore A^{+}_{Os}(Y_O\cos\phi_O - Y_1\cos\phi_1) = A^{-}_{Os}(Y_1\cos\phi_1 + Y_O\cos\phi_O)$$

$$\therefore A^{-}_{Os} = \frac{Y_O\cos\phi_O - Y_1\cos\phi_1}{Y_1\cos\phi_1 + Y_O\cos\phi_O} \cdot A^{+}_{Os} \qquad \text{---- (2.1.14)}$$

Similarly from equations (2.1.13a) and (2.1.13d),

$$(A^{+}_{Op} + A^{-}_{Op}).Y_O = (A^{+}_{Op} - A^{-}_{Op}) \cdot \frac{\cos\phi_O}{\cos\phi_1} \cdot Y_1$$

$$\therefore (A^{+}_{Op} + A^{-}_{Op}).Y_O\cos\phi_1 = (A^{+}_{Op} - A^{-}_{Op}).Y_1\cos\phi_O$$

$$\therefore A^{-}_{Op}(Y_O\cos\phi_1 + Y_1\cos\phi_O) = A^{+}_{Op}(Y_1\cos\phi_O - Y_O\cos\phi_1)$$

$$\therefore A^{-}_{Op} = \frac{Y_1\cos\phi_O - Y_O\cos\phi_1}{Y_O\cos\phi_1 + Y_1\cos\phi_O} \cdot A^{+}_{Op} \qquad \text{---- (2.1.15)}$$

and hence,

$$A^{+}_{1s} = A^{+}_{Os} + A^{-}_{Os} = \frac{2Y_O\cos\phi_O}{Y_O\cos\phi_O + Y_1\cos\phi_1} \cdot A^{+}_{Os} \qquad \text{---- (2.1.16)}$$

$$A^{+}_{1p} = (A^{+}_{Op} + A^{-}_{Op}) \frac{\cos\phi_0}{\cos\phi_1} = \frac{2Y_0 \cos\phi_0}{Y_0\cos\phi_1 + Y_1\cos\phi_0} \cdot A^{+}_{Op} \quad \text{---- (2.1.17)}$$

Equation (2.1.14) can be written as

$$A^{-}_{Os} = \frac{\cos\phi_0 - \frac{Y_1}{Y_0}\cos\phi_1}{\cos\phi_0 + \frac{Y_1}{Y_0}\cos\phi_1} \cdot A^{+}_{Os}$$

$$= \frac{\sin\phi_1 \cos\phi_0 - \sin\phi_0 \cos\phi_1}{\sin\phi_1 \cos\phi_0 + \sin\phi_0 \cos\phi_1} \cdot A^{+}_{Os}$$

since

$$\frac{Y_1}{Y_0} = \frac{n_1}{n_0} = \frac{\sin\phi_0}{\sin\phi_1}$$

from Snell's Law,

$$= -\frac{\sin(\phi_0 - \phi_1)}{\sin(\phi_0 + \phi_1)} \cdot A^{+}_{Os} \quad \text{---- (2.1.18)}$$

and similarly for equations (2.1.15), (2.1.16), (2.1.17), giving

$$A^{+}_{1s} = \frac{2\sin\phi_1 \cos\phi_0}{\sin(\phi_0 + \phi_1)} \cdot A^{+}_{Os} \quad \text{---- (2.1.19)}$$

$$A^{-}_{Op} = \frac{\tan(\phi_0 - \phi_1)}{\tan(\phi_0 + \phi_1)} \cdot A^{+}_{Op} \quad \text{---- (2.1.20)}$$

$$A^{+}_{1p} = \frac{2\sin\phi_1 \cos\phi_0}{\sin(\phi_0 + \phi_1)\cos(\phi_0 - \phi_1)} \cdot A^{+}_{Op} \quad \text{---- (2.1.21)}$$

Equations (2.1.18) to (2.1.21) are called the Fresnel formulae being first derived by Fresnel in 1823. From equation (2.1.20) when the value of $\phi_0 + \phi_1$ is $\pi/2$, it is seen that $A^{-}_{Op} = 0$. The angle of incidence at which this /

this occurs is called the polarizing angle, the result being called Brewster's Law, where the electric field strength vector of the reflected light has no component in the plane of incidence.

Since

$$\sin\phi_1 = \sin(\frac{\pi}{2} - \phi_0) = \cos\phi_0$$

Snell's Law yields

$$\tan\phi_{0p} = n_{01} \qquad \text{---- (2.1.22)}$$

where ϕ_{0p} is the polarizing angle.

Figure 2.2 illustrates the variation of phase and the amplitude reflection coefficients r_{01}^{s} and r_{01}^{p} with angle of incidence when $r_{01}^{s} = A_{0s}^{-}/A_{0s}^{+}$ and $r_{01}^{p} = A_{0p}^{-}/A_{0p}^{+}$. For an angle of incidence greater than the Brewster angle r_{01}^{p} changes sign and becomes positive.

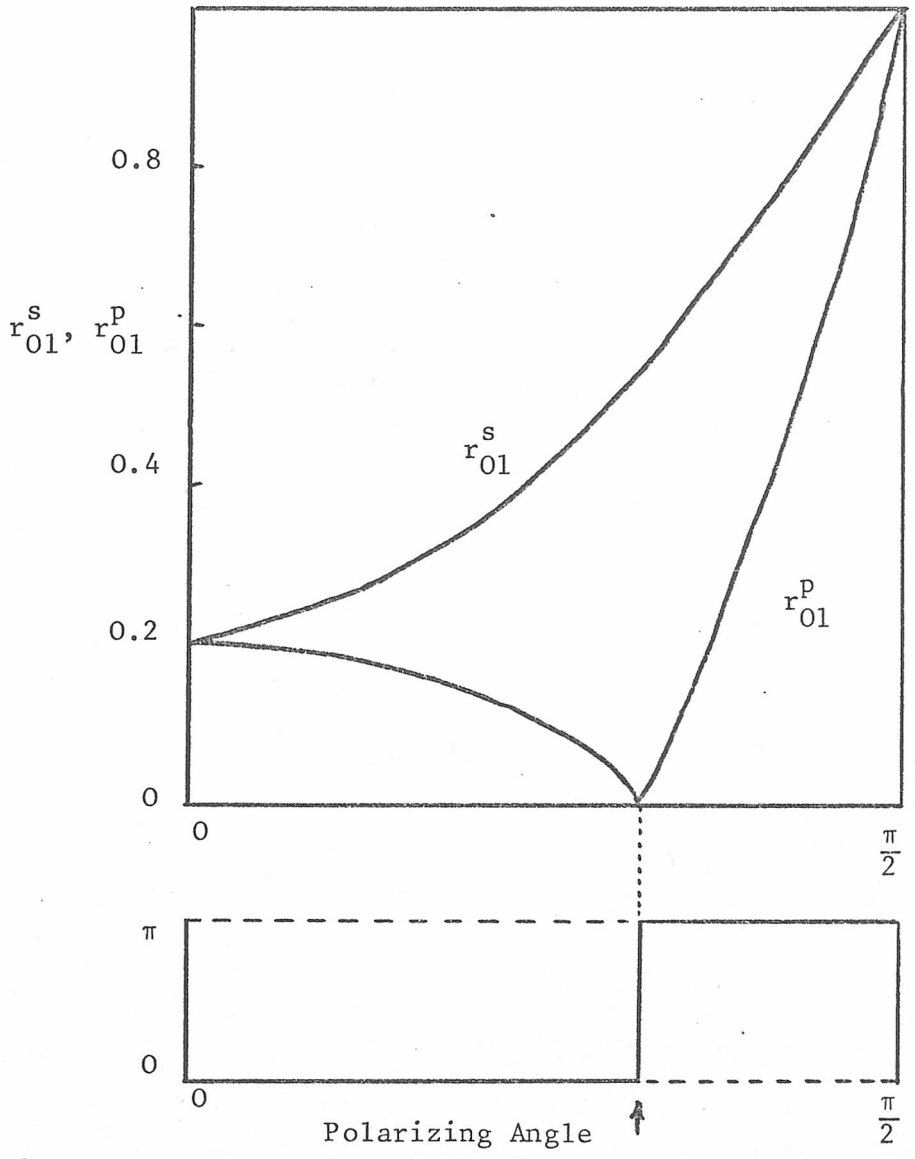

Figure 2.2 Variation with angle of incidence of phase Δ and reflection amplitude coefficients r_{01}^s and r_{01}^p for a dielectric, illustrating the phase change at the Polarizing Angle.

2.2.0 Reflection and Refraction of Light Through a Thin Homogeneous Dielectric Film

2.2.1 The Resultant Reflection and Transmission Amplitude Coefficients

In Section 2.1.3 the Fresnel or amplitude reflection and transmission coefficients were defined for both s and p - polarisation by equations (2.1.14) to (2.1.17). Hence at the air-film boundary described by Figure 2.3(a) the reflection and transmission amplitude coefficients are given as:

$$r_{01}^{s} = A_{0s}^{-}/A_{0s}^{+} = (Y_0\cos\phi_0 - Y_1\cos\phi_1)/(Y_1\cos\phi_1 + Y_0\cos\phi_0) \quad \text{---- (2.2.1a)}$$

$$r_{01}^{p} = A_{0p}^{-}/A_{0p}^{+} = (Y_1\cos\phi_0 - Y_0\cos\phi_1)/(Y_0\cos\phi_1 + Y_1\cos\phi_0) \quad \text{---- (2.2.2a)}$$

$$t_{01}^{s} = A_{1s}^{+}/A_{0s}^{+} = 2Y_0\cos\phi_0/(Y_0\cos\phi_0 + Y_1\cos\phi_1) \quad \text{---- (2.2.3a)}$$

$$t_{01}^{p} = A_{1p}^{+}/A_{0p}^{+} = 2Y_0\cos\phi_0/(Y_0\cos\phi_1 + Y_1\cos\phi_0) \quad \text{---- (2.2.4a)}$$

Similarly at the film-substrate boundary:

$$r_{12}^{s} = (Y_1\cos\phi_1 - Y_2\cos\phi_2)/(Y_2\cos\phi_2 + Y_1\cos\phi_1) \quad \text{---- (2.2.1b)}$$

$$r_{12}^{p} = (Y_2\cos\phi_1 - Y_1\cos\phi_2)/(Y_1\cos\phi_2 + Y_2\cos\phi_1) \quad \text{---- (2.2.2b)}$$

$$t_{12}^{s} = 2Y_1\cos\phi_1/(Y_1\cos\phi_1 + Y_2\cos\phi_2) \quad \text{---- (2.2.3b)}$$

$$t_{12}^{p} = 2Y_1\cos\phi_1/(Y_1\cos\phi_2 + Y_2\cos\phi_1) \quad \text{---- (2.2.4b)}$$

Using /

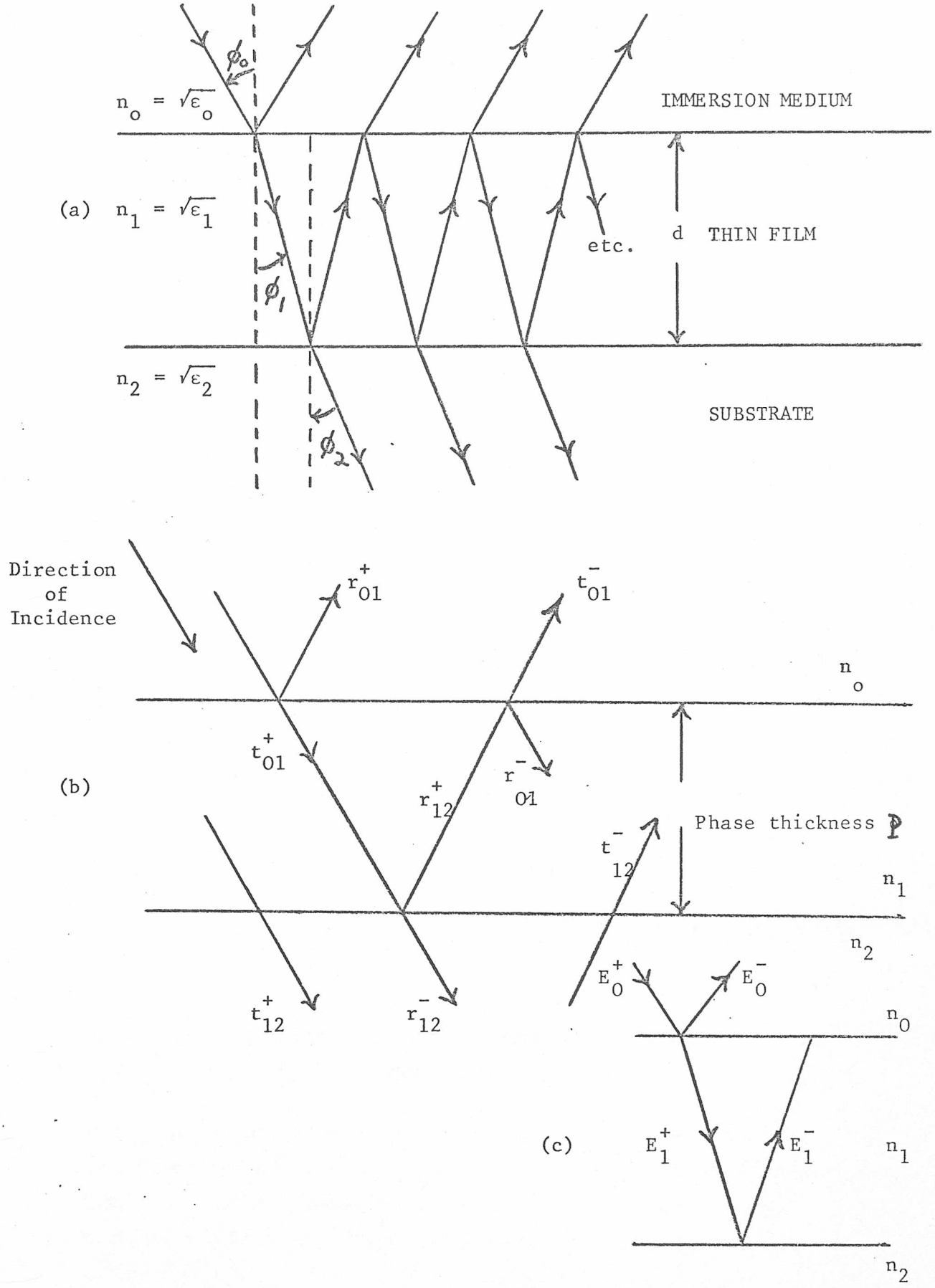

Figure 2.3 Reflection and refraction of light through a thin homogeneous film, illustrating (a) general notations (b) reflection and transmission amplitude coefficients (c) electric field vectors.

Using Figure 2.3b to define the various parameters involved, and dropping the s and p notation since the outcome is valid for either, it is seen that the incident wave will first of all be partially reflected at the first interface. The remainder of the wave will pass into the film and will be reflected successively at the second and first interfaces, a fraction being transmitted through the appropriate interface each time. Hence the amplitudes of the transmitted and reflected waves can be found by summing the separate fractions. The resultant amplitude reflection coefficient is given by:

$$R^{+} = r^{+}_{01} + t^{+}_{01}.r^{+}_{12}.t^{-}_{01}.\exp(-2iP) + t^{+}_{01}.r^{+}_{12}.r^{-}_{01}.r^{+}_{12}.t^{-}_{01}.\exp(-4iP) + t^{+}_{01}.r^{+}_{12}.r^{-}_{01}.r^{+}_{12}.r^{-}_{01}.r^{+}_{12}.t^{-}_{01}.\exp(-6iP) + \ldots\ldots\ldots\ldots\ldots$$

$$= r^{+}_{01} + t^{+}_{01}.r^{+}_{12}.t^{-}_{01}.\exp(-2iP)\,[1/1-r^{-}_{01}.r^{+}_{12}.\exp(-2iP)] \qquad \text{---- (2.2.5)}$$

which is the solution of a geometric progression of common ratio $r^{-}_{01}.r^{+}_{12}.\exp(-2iP)$.

The amplitude damping factor exp(-D) is due to the attenuation of the medium. D is the phase difference between light beams reflected from the immersion medium - film and film-substrate boundaries and is given by

$$D = 2iP = 4\pi i n_1 \, d \cos\phi_1/\lambda \qquad \text{---- (2.2.6)}$$

where n_1 is the refractive index and d the physical thickness of the film, and λ is the wavelength of light used.

From /

From equation (2.2.3a),

$$t_{01}^{+} = 2p_0/(p_0 + p_1) \quad \text{where } p = Y\cos\phi$$

and by symmetry

$$t_{01}^{-} = 2p_1/(p_0 + p_1)$$

Similarly from equation (2.2.1a),

$$r_{01}^{+} = (p_0 - p_1)/(p_0 + p_1)$$

Hence $t_{01}^{+} \cdot t_{01}^{-} = \dfrac{4p_0\, p_1}{(p_0+p_1)^2}$

$$= \frac{p_0^{\,2} + 2p_0p_1 + p_1^{\,2} - p_0^{\,2} + 2p_1p_0 - p_1^{\,2}}{(p_0 + p_1)^2}$$

$$= 1 - \frac{(p_0^{\,2} - 2p_0p_1 + p_1^{\,2})}{(p_0 + p_1)^2}$$

$$= 1 - (r_{01}^{+})^2 \qquad \text{---- (2.2.7)}$$

Using equation (2.2.7) and the fact that $r_{01}^{-} = -r_{01}^{+}$ in equation (2.2.5) gives:

$$R^{+} = r_{01}^{+} + \frac{r_{12}^{+} \cdot \exp(-D)\,[1 - (r_{01}^{+})^2]}{1 + r_{01}^{+} \cdot r_{12}^{+} \cdot \exp(-D)}$$

$$= r_{01}^{+} + \frac{r_{12}^{+}\cdot\exp(-D) - r_{12}^{+}\cdot(r_{01}^{+})^2 \cdot \exp(-D)}{1 + r_{01}^{+}\cdot r_{12}^{+}\cdot\exp(-D)}$$

$$= /$$

$$= \frac{r_{01}^{+} + (r_{01}^{+})^2 \cdot r_{12}^{+} \cdot \exp(-D) + r_{12}^{+} \cdot \exp(-D) - r_{12}^{+} \cdot (r_{01}^{+})^2 \exp(-D)}{1 + r_{01}^{+} \cdot r_{12}^{+} \cdot \exp(-D)}$$

$$= \frac{r_{01}^{+} + r_{12}^{+} \cdot \exp(-D)}{1 + r_{01}^{+} \cdot r_{12}^{+} \cdot \exp(-D)} \qquad \text{---- (2.2.8)}$$

The resultant amplitude transmission coefficient is derived similarly:

$$T^{+} = t_{01}^{+} \cdot t_{12}^{+} \cdot \exp(-iP) + t_{01}^{+} \cdot r_{12}^{+} \cdot r_{01}^{-} \cdot t_{12}^{+} \cdot \exp(-3iP)$$

$$+ \; t_{01}^{+} \cdot r_{12}^{+} \cdot r_{01}^{-} \cdot r_{12}^{+} \cdot r_{01}^{-} \cdot t_{12}^{+} \cdot \exp(-5iP)$$

$$+ \; \ldots\ldots\ldots$$

which is a geometric progression and reduces to

$$T^{+} = \frac{t_{01}^{-} \cdot t_{12}^{+} \cdot \exp(-iP)}{1 - r_{01}^{-} \cdot r_{12}^{+} \cdot \exp(-2iP)}$$

$$= \frac{t_{01}^{+} \cdot t_{12}^{+} \cdot \exp(-iP)}{1 + r_{01}^{+} \cdot r_{12}^{+} \cdot \exp(-2iP)} \qquad \text{---- (2.2.9)}$$

By successive application the above expressions (2.2.8) and (2.2.9) can be extended to a stratified medium. The matrix approach as developed by Born and Wolf (1970) is an alternative method of derivation of R^{+} and T^{+}, which lends itself directly to computation. Hence a characteristic matrix, which in this case is given in terms of the electric field strengh vectors (Figure 2.3c), could be expressed as:

$$\begin{bmatrix} E_0^{+} \\ E_0^{-} \end{bmatrix} = \frac{1}{t_{01}^{+}} \begin{bmatrix} \exp(iP) & r_{01}^{+} \cdot \exp(iP) \\ r_{01}^{+} \cdot \exp(-iP) & \exp(-iP) \end{bmatrix} \begin{bmatrix} E_1^{+} \\ E_1^{-} \end{bmatrix} \qquad \text{---- (2.2.10)}$$

(MacLeod (1969))

2.3.0 Polarized Light

2.3.1 Types of Polarized Light

If the direction of the transverse electric field strength vector, which it is thought excites perception of light in the eye (Vašíček 1960), is constant in time, the wave is then linearly or plane polarized and is the simplest component into which light can be decomposed. Hence any complicated electromagnetic wave can be built up from individual plane waves of the same frequency with differing amplitude, orientation and phase, all propagating in the same direction.

With linearly polarized waves the electric field strength vector always lies in a given direction, however the most general type of polarization is elliptic polarization which includes the other two types (linear and circular) as special cases. Elliptically polarized light is the result of a combination of two uniform plane waves of the same frequency but of different magnitudes, phases and orientations of the field vectors.

Each type of polarization is characterised by polarization forms. Linear polarization has an infinite number of polarization forms, differing solely as to azimuth (the angle between the plane of polarization and the reference plane). Circular polarization however has two forms differing as to the direction in which the electric vector rotates, being either right or left handed. Elliptic polarization has an infinite number of forms, differing in direction of rotation, azimuth and ellipticity (the ratio of minor to major axes of the ellipse).

2.3.2 /

2.3.2 Mathematical Description of Polarized Light

Modern methods of specifying polarized light can provide a direct insight into calculations involving the influence of polarizers and retarders upon a wave. These somewhat specialised methods which include the Poincaré sphere, the Stokes vector, the Jones vector and the Mueller calculus, are described by Shurcliff (1962), however only the classical derivation will be considered here.

In the coordinate system adopted in Figure 2.1 let the angle contained by the magnetic field strength vector $\vec{H}$ and the plane of incidence be denoted as Θ. The components of the electric field vector $\vec{E}$ in the coordinate axes are therefore given by

$$E_p = E \sin\Theta \qquad \text{---- (2.3.1a)}$$

$$E_s = E \cos\Theta \qquad \text{---- (2.3.1b)}$$

Two arbitrary vibrations with the same frequency and amplitudes A and B, parallel to the two coordinate axes, can be represented as

$$E_p = A \cos(\omega t+\delta_p) \qquad \text{---- (2.3.2a)}$$

$$E_s = B \cos(\omega t+\delta_s) \qquad \text{---- (2.3.2b)}$$

If $\Delta = \delta_p - \delta_s$ then when the two vibrations are in phase ($\Delta = 0$) or in opposite phase ($\Delta = \pm\pi$), the ratio of equation (2.3.2) is

$$\frac{E_p}{E_s} = \pm \frac{A}{B} \qquad \text{---- (2.3.3)}$$

which is the equation of a straight line in the X-Y plane. Hence /

Hence the light is linearly polarized. In general however, Δ is arbitrary and from equation (2.3.2) we get,

$$\left(\frac{E_p}{A}\right)^2+\left(\frac{E_s}{B}\right)^2 = \cos^2(\omega t+\delta_p) + \cos^2(\omega t+\delta_s)$$

$$= \tfrac{1}{2}(1 + \cos 2(\omega t+\delta_p)) + \tfrac{1}{2}(1 + \cos 2(\omega t+\delta_s))$$

$$= 1 + \tfrac{1}{2}[\cos 2(\omega t+\delta_p) + \cos 2(\omega t+\delta_s)]$$

$$= 1 + \tfrac{1}{2}[2\cos(2\omega t + (\delta_p+\delta_s))\cos\Delta]$$

$$= 1 + \cos[(2\omega t + (\delta_p+\delta_s)]\cos\Delta$$

$$= 1 + \cos[(\omega t+\delta_p) + (\omega t+\delta_s)]\cos\Delta$$

$$= 1 + [\cos(\omega t+\delta_p)\cos(\omega t+\delta_s) - \sin(\omega t+\delta_p)\sin(\omega t+\delta_s)]\cos\Delta$$

$$= 1 + [2\cos(\omega t+\delta_p)\cos(\omega t+\delta_s)]\cos\Delta - \cos\Delta[\cos(\omega t+\delta_p)\cos(\omega t+\delta_s) + \sin(\omega t+\delta_p)\sin(\omega t+\delta_s)]$$

$$= 1 + 2\cos(\omega t+\delta_p)\cos(\omega t+\delta_s)\cos\Delta - \cos\Delta[\cos(\omega t+\delta_p-\omega t-\delta_s)]$$

$$= 1 + 2\cos(\omega t+\delta_p)\cos(\omega t+\delta_s)\cos\Delta - \cos\Delta\cos\Delta$$

$$= \sin^2\Delta + 2\cos(\omega t+\delta_p)\cos(\omega t+\delta_s)\cos\Delta$$

$$= \sin^2\Delta + 2\left(\frac{E_p}{A}\right)\left(\frac{E_s}{B}\right)\cos\Delta$$

ie $$\left(\frac{E_p}{A}\right)^2+\left(\frac{E_s}{B}\right)^2 - 2\left(\frac{E_p}{A}\right)\left(\frac{E_s}{B}\right)\cos\Delta = \sin^2\Delta \quad \text{---- (2.3.4)}$$

which is the equation of an ellipse.

The locus of the light vector traces out an ellipse that is inscribed in a rectangle of dimensions 2A, 2B as shown in Figure 2.4, the semi-axes of which do not coincide with equation (2.3.4). We can, however, introduce a new coordinate system (ξ,η) and from the theory of linear transformations it is known that the rotation is given by

$$E_\xi = E_p \cos\chi + E_s \sin\chi \qquad \text{---- (2.3.5a)}$$

$$E_\eta = -E_p \sin\chi + E_s \cos\chi \qquad \text{---- (2.3.5b)}$$

where χ is the angle between the major semi-axis of the ellipse and the x-axis. In the new coordinate system the ellipse is described by

$$E_\xi = a \cos(\omega t+\delta_o) \qquad \text{---- (2.3.6a)}$$

$$E_\eta = \pm b \sin(\omega t+\delta_o) \qquad \text{---- (2.3.6b)}$$

where a and b are the semi-axes of the ellipse. The double sign in equation (2.3.6b) is introduced so that the two possible ellipticities (positive or negative) can be taken into consideration. Vasicek (1960) shows that by substituting equation (2.3.2) into equation (2.3.5), and setting equations (2.3.5) and (2.3.6) equal the following is obtained:

$$\begin{aligned} a(\cos\omega t \cos\delta_o - \sin\omega t \sin\delta_o) &= A(\cos\omega t \cos\delta_p - \sin\omega t \sin\delta_p)\cos\chi \\ &\quad + B(\cos\omega t \cos\delta_s - \sin\omega t \sin\delta_s)\sin\chi \end{aligned} \qquad \text{---- (2.3.7)}$$

$$\begin{aligned} \pm b(\sin\omega t \cos\delta_o + \cos\omega t \sin\delta_o) &= -A(\cos\omega t \cos\delta_p - \sin\omega t \sin\delta_p)\sin\chi \\ &\quad + B(\cos\omega t \cos\delta_s - \sin\omega t \sin\delta_s)\cos\chi \end{aligned} \qquad \text{---- (2.3.8)}$$

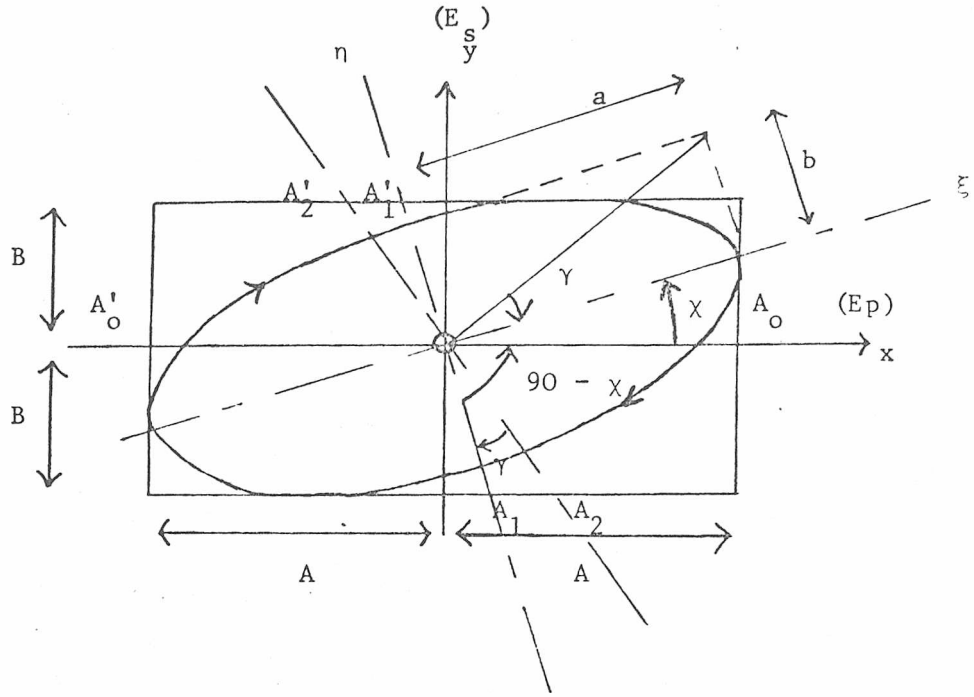

Figure 2.4 The Vibrational Ellipse for the Electric Field Strength Vector.

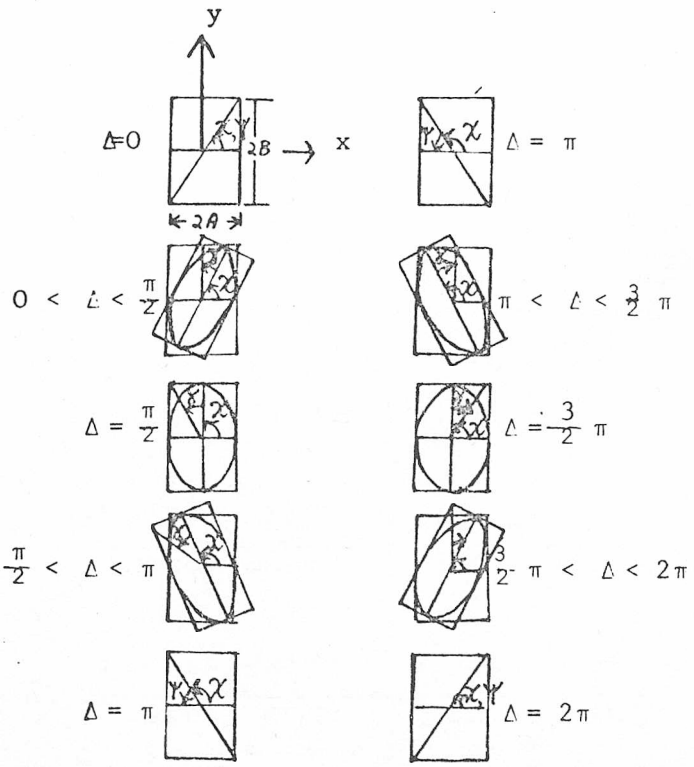

Figure 2.5 Dependence of Elliptic Polarization on the Phase Difference Δ between Orthogonal Linearly Polarized Components of Amplitude A and B (Muller, 1969).

Comparing $\sin\omega t$ and $\cos\omega t$ terms gives

$$a\cos\delta_o = A\cos\delta_p\cos\chi + B\cos\delta_s\sin\chi \quad \text{---- (2.3.9a)}$$

$$a\sin\delta_o = A\sin\delta_p\cos\chi + B\sin\delta_s\sin\chi \quad \text{---- (2.3.9b)}$$

and

$$\pm b\cos\delta_o = +A\sin\delta_p\sin\chi - B\sin\delta_s\cos\chi \quad \text{---- (2.3.10a)}$$

$$\pm b\sin\delta_o = -A\cos\delta_p\sin\chi + B\cos\delta_s\cos\chi \quad \text{---- (2.3.10b)}$$

Squaring equations (2.3.9) and (2.3.10) and adding produces

$$a^2 = A^2\cos^2\chi + B^2\sin^2\chi + 2AB\cos\Delta\cos\chi\sin\chi \quad \text{---- (2.3.11a)}$$

$$b^2 = A^2\sin^2\chi + B^2\cos^2\chi - 2AB\cos\Delta\cos\chi\sin\chi \quad \text{---- (2.3.11b)}$$

where $\Delta = \delta_p - \delta_s$. Hence the relation between the semi-axes of the ellipse and the amplitudes of vibration is

$$a^2 + b^2 = A^2 + B^2 \quad \text{---- (2.3.12)}$$

and by dividing equation (2.3.10a) by equation (2.3.9a) and similarly with (2.3.10b) and (2.3.9b) the ratio of the semi-axes is given by

$$\pm\frac{b}{a} = \frac{A\sin\delta_p\sin\chi - B\sin\delta_s\cos\chi}{A\cos\delta_p\cos\chi + B\cos\delta_s\sin\chi}$$

$$= \frac{-A\cos\delta_p\sin\chi + B\cos\delta_s\cos\chi}{A\sin\delta_p\cos\chi + B\sin\delta_s\sin\chi} \quad \text{---- (2.3.13)}$$

ie, /

ie,

$$(A\sin\delta_p \sin\chi - B\sin\delta_s \cos\chi)(A\sin\delta_p \cos\chi + B\sin\delta_s \sin\chi)$$

$$= (-A\cos\delta_p\sin\chi + B\cos\delta_s\cos\chi)(A\cos\delta_p \cos\chi + B\cos\delta_s \sin\chi)$$

$$\therefore A^2\sin^2\delta_p\cos\chi\sin\chi - AB\sin\delta_p\sin\delta_s \cos^2\chi$$
$$+ AB \sin\delta_p\sin\delta_s\sin^2\chi - B^2\sin^2\delta_s\cos\chi \sin\chi$$

$$= -A^2\cos^2\delta_p \sin\chi \cos\chi + AB \cos\delta_p \cos\delta_s \cos^2\chi$$
$$- AB \cos\delta_p \cos\delta_s \sin^2\chi + B^2 \cos^2\delta_s \cos\chi \sin\chi$$

$$\therefore A^2\sin\chi \cos\chi(\sin^2\delta_p+\cos^2\delta_p) - B^2 \sin\chi \cos\chi(\sin^2\delta_s+\cos^2\delta_s)$$

$$= AB \sin\delta_p \sin\delta_s(\cos^2\chi-\sin^2\chi) + AB \cos\delta_p\cos\delta_s(\cos^2\chi-\sin^2\chi)$$

$$\therefore (A^2-B^2)\sin\chi \cos\chi = AB \cos2\chi(\cos\delta_p\cos\delta_s+\sin\delta_p\cos\delta_s)$$

$$\therefore (A^2-B^2)\sin2\chi = 2AB \cos2\chi \cos\Delta \quad \text{---- (2.3.14)}$$

If the ratio of the amplitudes is denoted as

$$\frac{B}{A} = \tan\psi \quad \text{---- (2.3.15)}$$

where ψ is the azimuth, then from equation (2.3.14)

$$\tan 2\chi = \frac{2AB\cos\Delta}{A^2 - B^2}$$

$$= \frac{2\tan\psi \cos\Delta}{1 - \tan^2\psi}$$

ie

$$\tan 2\chi = \tan 2\psi \cos\Delta \quad \text{---- (2.3.16)}$$

Furthermore, /

Furthermore, if the ratio of the semi-axes of the ellipse is denoted by

$$\frac{b}{a} = \tan \gamma \qquad \text{---- (2.3.17)}$$

where γ is termed the ellipticity, shown in equation (2.3.13) to be either positive or negative, and by multiplying equation (2.3.9a) by (2.3.10a) and equation (2.3.9b) by (2.3.10b), then adding gives

$$\pm ab = AB \sin\Delta \qquad \text{---- (2.3.18)}$$

Therefore from equations (2.3.12), (2.3.17) and (2.3.18) is produced

$$\sin 2\gamma = \frac{2ab}{a^2 + b^2}$$

$$= \pm \frac{2AB \sin\Delta}{A^2 + B^2}$$

ie

$$\sin 2\gamma = \pm \sin 2\psi \sin\Delta \qquad \text{---- (2.3.19)}$$

From equations (2.3.16) and (2.3.19) can be derived expressions for the angle ψ and the phase difference Δ, Figure 2.5 showing clearly the dependence of elliptic polarization on Δ.

Hence it is seen that the ellipse, first characterised from physical reasoning by ψ, the azimuth, and Δ, the phase difference of the p and s components, can also, from geometrical considerations, be characterised by χ, the inclination of the major axis to the plane of incidence, and by the ellipticity γ given by the ratio of minor to major axis in equation (2.3.17).

2.3.3 /

2.3.3 The Basic Equation of Ellipsometry

Relative changes in amplitude ratio, ψ, and phase of a light beam, Δ, can be conveniently studied by reflecting a polarized light beam from the surface under investigation and analysing the changes in the polarization of the beam. These relative changes can be expressed by the ratio of the resultant reflection amplitude coefficients (equation (2.2.8)) for the p and s polarization, resulting in the fundamental equation of ellipsometry:

$$\frac{R_p^+}{R_s^+} = \frac{|r_p| \exp(i\delta_p)}{|r_s| \exp(i\delta_s)}$$

$$= \frac{|r_p|}{|r_s|} \exp\left[i(\delta_p - \delta_s)\right]$$

$$= \tan\psi \cdot \exp(i\Delta)$$

$$= Q \qquad \text{---- (2.3.20)}$$

where the factor Q is called the complex relative amplitude attenuation (Muller, 1969). The ellipsometer measures the experimental quantities, χ and γ, that allow the determination of ψ and Δ as will be shown later.

CHAPTER 3

CONSTRUCTION OF AN ELLIPSOMETER

The ellipsometer (see Plate 1) is an instrument which facilitates the calculation of the thickness and optical constants of thin, dielectric or absorbing films by the analysis of elliptically polarized light reflected from the film on a reflecting substrate. Bennett and Bennett (1967) point out that although there may appear to be an unlimited number of ways in which ellipsometric measurements can be made, they basically fall into five categories, one of which is outlined here as a quick, accurate method of determining the characteristic γ and χ values, provided that the extinction position is easily determined. The schematic representation of this method is shown in Figure 3.1, with the wave plate on the emergent arm, although the optical equivalent (ie, wave plate on the incident arm) is equally valid.

3.1.0 The Optical System

The two arms of the optical system are mounted on optical benches which are rotatable in a horizontal plane about the same vertical axis. Attached to the turntable (T), which can also rotate about the common vertical axis, is a sample holder (Plate 2), which accepts rectangular or circular samples. The sample holder can move so that the face of the sample is directly above the axis of rotation and lies in the same vertical plane.

3.1.1 The Incident Arm

The purpose of the incident arm is to provide an incident beam of parallel, plane-polarized and monochromatic light at the sample surface.

The /

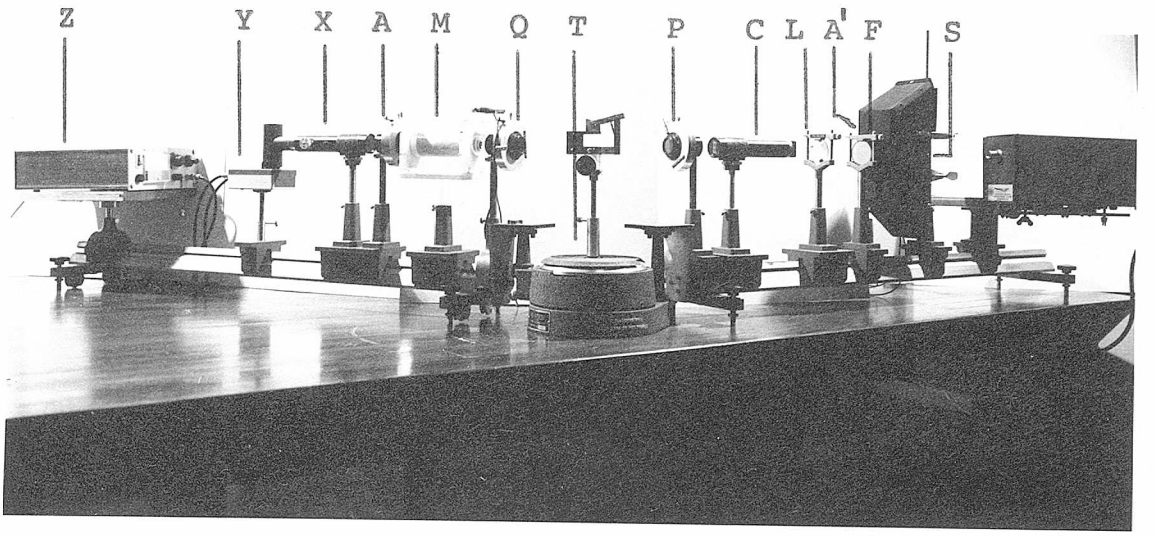

Plate 1 The Ellipsometer

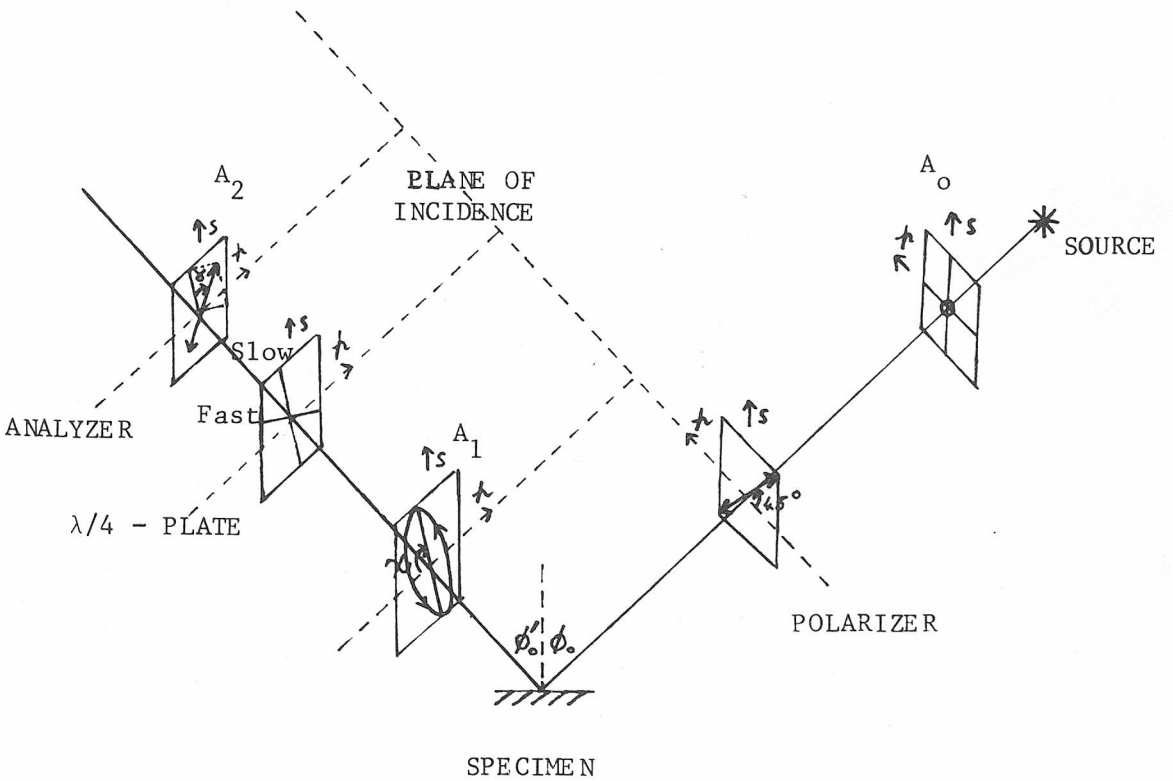

Figure 3.1 The Optical System Schematic

The light source (S in Figure 3.1) is a d.c. stabilized 150W tungsten halogen lamp, mounted with a parabolic mirror behind and enclosed in a suitable housing (Plate 3). The iris aperture (A') is fitted on the lamp housing and limits the surface area of the beam before it passes through an interference filter (F) for 5461 Å wavelength, having a bandwidth of 140 Å and 50 percent transmittance. A convex lens (L) focuses the image of the lamp filament on to the collimator entrance slit (c). The polarizer (p) is mounted vertically in a divided circle with a vernier reading to 0.05 degrees.

3.1.2 The Emergent Arm

The emergent arm analyses the elliptically polarized light reflected by the sample surface.

The reflected beam passes through the retarder (Q), which like the polarizer and analyser is mounted in a vertical divided circle reading to 0.05 degrees. Modulation of the beam is then achieved by a Faraday modulator (M) before it is passed through the analyser (A) and the telescope (X) to be detected by the photomultiplier (Y). The photomultiplier, which is connected to a 0-2kV power supply (Z) and an oscilloscope, can be removed for visual alignment purposes.

3.1.3 The Polarizer and Analyzer

There are several different ways of producing polarized light directly, however these are of little practical importance being derived from the Čerenkov, Stark, Zeeman and other effects, biemissivity, bifluorescence and grazing emergence. The normal method in practice is to utilise a polarizer to polarize light from a source by eliminating one component and transmitting the orthogonal component.

For /

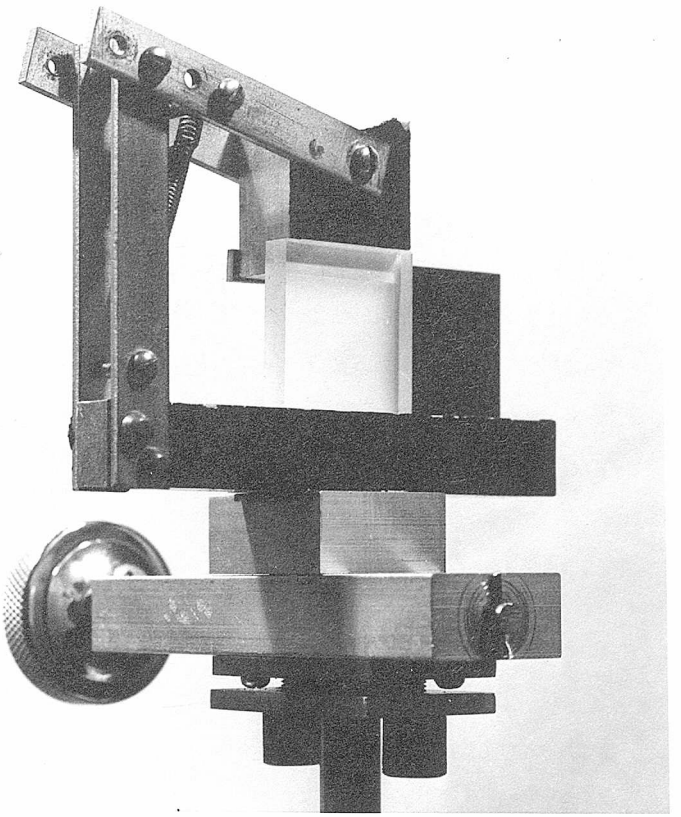

Plate 2 The Sample Holder.

Plate 3 The Lamp Housing.

For ellipsometry, as in many other optical systems, two polarizers are used - one produces the polarization, and the other usually termed the analyzer (although by itself it is not sufficient for a complete analysis) enables any modification in the polarization to be determined. There are three main classes of polarizer; birefringent, reflection and dichroic. Their comparative usefulness depends on the efficiency of the device, its angular acceptance, its wavelength range and its cost. King and Talim (1970) outline some aspects of polarizer performance using extinction ratio, axis wander and ellipticity of the emergent polarized beam as a measure of the criterion of efficiency.

The polarizers employed for the ellipsometer are POLAREX (Ks - MIK grade) filters of high polymeric colloid film, the molecules of which are orientated by mechanical stretching. The film is dyed grey and cemented between strain free protective glass, ground plane parallel to within 4 angular minutes and finely polished. For a 4mm diameter aperture at the polarizer and a separation of 20mm between the polarizer and photomultiplier, King and Talim (1970) showed that for perfectly linearly polarized light, produced by a combination of a sheet polarizer and Brewster angle reflector, the extinction ratio of the Ks-MIK filter was of the order of $1.0 - 2.6 \times 10^{-6}$, which compared favourably with conventional Glan-Thomson birefringent polarizers and significantly better than POLAROID (HN-22 and HN-32 grade) polarizers. Reflection polarizers are unsuitable for ellipsometry but are used successfully in infrared spectrophotometry. The cost factor, large acceptance angle and comparable extinction ratio justified the use of the Ks-MIK sheet polarizer over a prism polarizer despite a lower transmission of the wanted component.

Since /

Since the polarizer is not perfectly homogeneous due to scattering and strain from the mounting, the emergent face which results in the greatest degree of polarization is designated the prime face. For the analyzer the prime face is the incident face and opposes the prime face of the polarizer in the ellipsometer.

3.1.4 The Wave Plate

A retarder converts a polarization form by resolving the light beam into two components, retarding the phase of one component relative to the other before combining the components again, without changing the degree of polarization or indeed the intensity. The amount of phase retardation is often termed the retardance and is expressed in terms of cycles, the most common linear retarders being the quarter-wave ($\lambda/4$) and half-wave ($\lambda/2$) plates. Birefringent retarders which are commonly referred to as wave plates, typically consist of a single plate of mica, quartz or calcite, or a sheet of oriented cellophane or polyvinyl alcohol, whereas reflection retarders utilise the fact that total internal reflection produces a component phase change, typical examples being the Fresnel and Mooney rhombs. Variable wave plates, known as compensators have retardances which vary from zero to a few waves, the most common being due to Babinet, Soleil and Senarmont.

An exact (to within 0.5 degrees) $\lambda/4$-plate is used in the ellipsometer since it is an efficient and cheap device consisting of an accurately turned mica plate, not mounted between cover glass in this case. The $\lambda/4$-plate is characterised by two fast and slow vibration eigenvectors, /

eigenvectors, which occur due to the relative speed of propagation in orthogonal directions of the plate. These, when aligned with the minor and major axes of the elliptically polarized light, result in plane polarized light. Mounting the $\lambda/4$-plate in the divided circles unfortunately gives rise to edge strains, causing polarization losses which can never be entirely avoided.

3.2.0 The Detection System

A null detection system is adopted for the ellipsometer since amplitude measurement is less precise. The simplest system is the use of a halfshade device like that used by Rothen (1945), where a number of barium stearate layers are deposited on the upper and lower part of the substrate before deposition of the film under investigation, such that the direction of polarization between the upper and lower part differs by approximately three degrees; the null position being then indicated, before and after the film deposition, by equal half-field intensity. Since the eye is a poor detector this tedious method has a limited sensitivity. If however a photomultiplier is substituted for the eye and a form of light beam modulation used instead of the halfshade device, a precision of ± 0.01 degrees in polarizer and analyzer settings can be achieved with suitable divided circles. The system used is outlined in Figure 3.2.

3.2.1 The Photomultiplier and Dynode Chain

Two completely different photomultipliers were considered; the 9 stage side window RCA-931A and the 13 stage end window EMI 6256B. The latter has a superior spectral response for 5461 Å wavelength, however /

however since the RCA-931A is a factor of ten cheaper, smaller in size, with comparatively high sensitivity and low dark current, it was used in the first instance. The tube is mounted on a suitable base and enclosed in a light-tight housing which fits onto the end of the telescope (see Plate 4). A cylinder of TELSHIELD magnetic shielding, in contact with the sides of the glass envelope, and at photocathode potential, is used to minimise the effect of environmental magnetic fields. In order to simplify the tube mounting from a safety point of view, the photocathode is grounded with the anode at a high positive potential delivered by a stabilised d.c. supply. The average anode current for the RCA-931A is rated as 1.0 mA (max.) the working voltage being optimised as 750V. The choice of resistance values for the dynode chain is a compromise between low values per stage resulting in a power drain or high values leading to a deviation from linearity. In practice the voltage divider current must be maintained at a value of at least ten times the maximum average anode current. Hence the standard dynode chain arrangement shown in Figure 3.3 is used with the value for R being 100 kΩ. The output of the photomultiplier is electric current which develops a voltage across the load resistance R_L which in turn is coupled to the oscilloscope via the capacitor C_C.

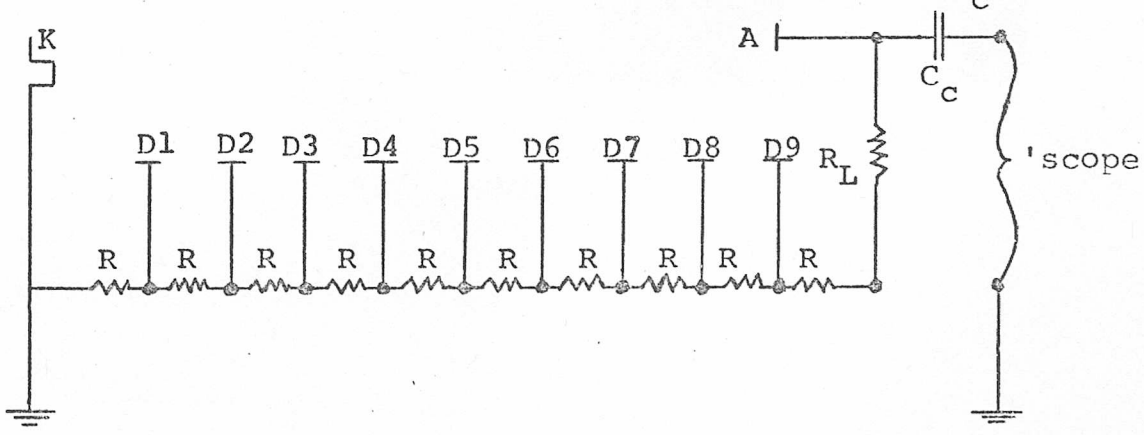

Figure 3.3 The standard dynode chain arrangement

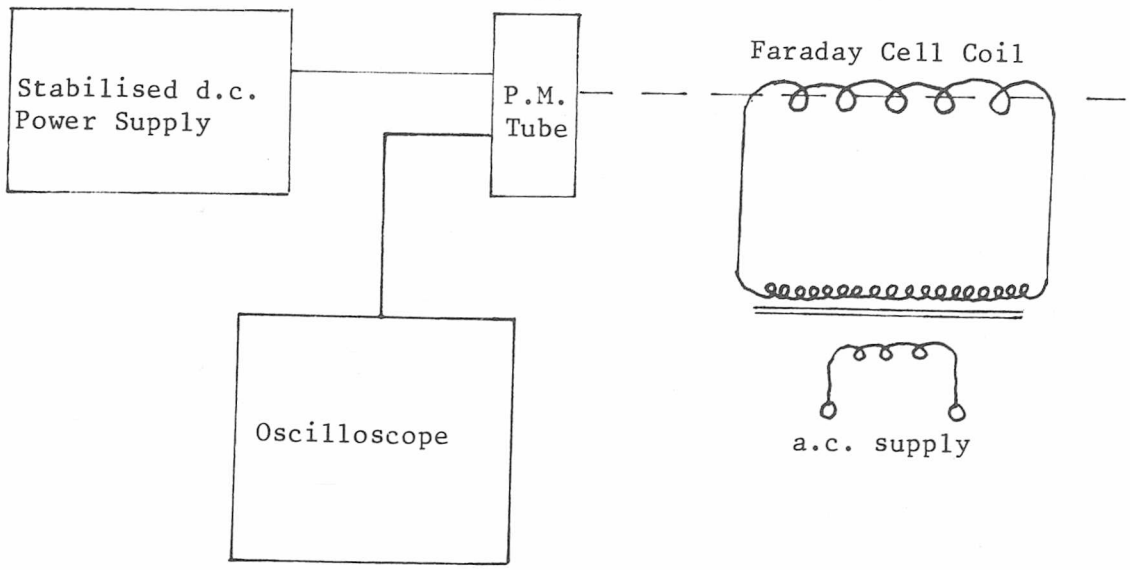

Figure 3.2 Schematic of the Detection System.

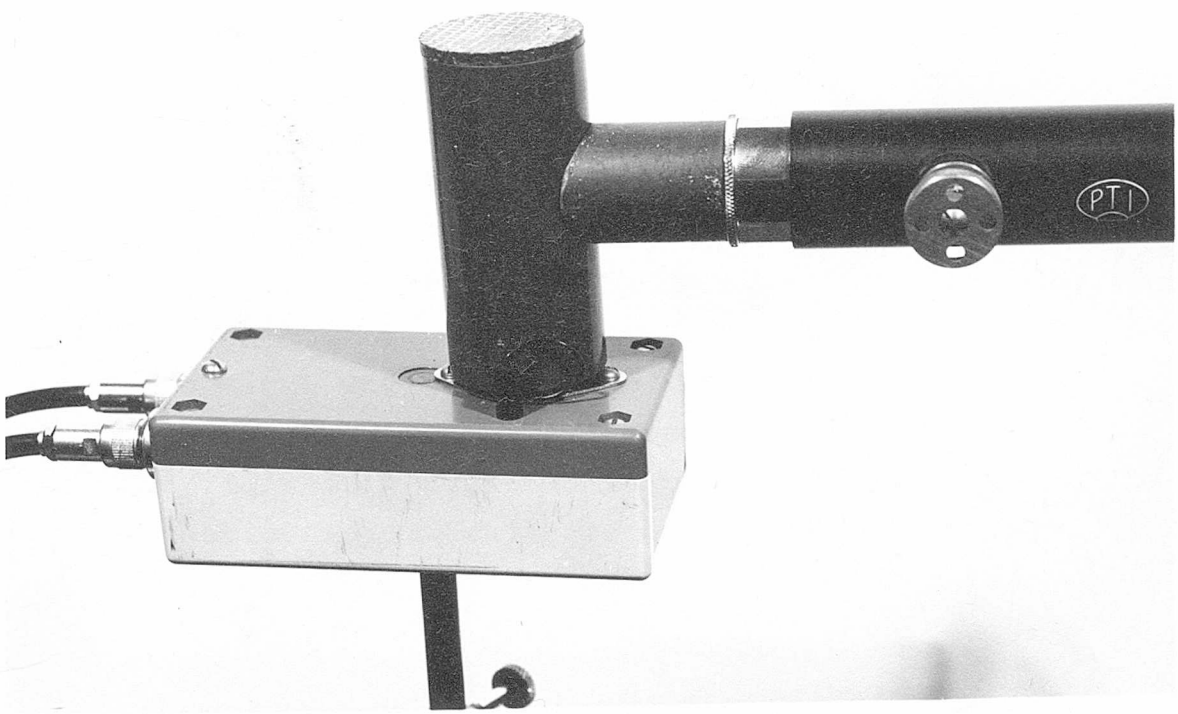

Plate 4 The Photomultiplier Housing.

3.2.2 Beam Modulation

Modulation of the beam can be effected by a mechanical chopper as in the Gaertner L-119 ellipsometer produced in USA (Smith 1969) or an optical device based upon electro- or magneto-optical phenomena. The chopper can lead to assymetry about the null position if the light is only partially polarized, the optical methods however, enable the polarizer and analyzer to be fixed, which is advantageous. The electro-optic effects, the Kerr effect in liquids and the Pockels effect in crystals, have not been used widely for ellipsometric applications, although Takasaki (1961) describes the use of a crystal of ADP (ammonium dihydrogen phosphate). The Faraday magnetic rotation of the plane of polarization enables sensitive setting of the polarizer and analyzer to be achieved and a Faraday modulator was constructed for this purpose.

3.2.3 The Faraday Modulator

The construction of a Faraday modulator is basically a two fold problem. There is the core, which can be solid or liquid and the solenoid, the design of which is somewhat dependent on the core. The interaction of light with the core substance involves the electronic structure of matter being affected by the magnetic state. The derivation of the effect from Maxwell's equations is described by Freiser (1968). The effect is a rotation of the plane of linearly polarized light through the core medium in a magnetic field. This causes the wave to be resolved into left and right circularly polarized components. For non-ferromagnetic materials this rotation is proportional to the applied magnetic field, the angle of rotation θ is given as

$$\theta = V \ell H = V \ell n i \qquad \text{---- (3.2.1)}$$

where /

where H is the magnetic field strength, ℓ is the length of the solenoid, i is the instaneous current, n the number of turns per unit length of solenoid and V is the Verdet constant and is a characteristic of the material. Specifications of several solenoids used in ellipsometry work and values of Verdet constants for some suitable core materials are given in a paper by Winterbottom (1964).

(a) The Core

The core material chosen for the modulator in this case is a cylindrical rod of Schott SF57 NSSK quality optical glass with a quoted residual stress birefringence of 2.0-3.0 Å per cm and antireflective end coatings. The low birefringence value enables higher currents to be used in the solenoid than normal, since there is less polarization loss due to core material temperature variation. The Verdet constant with 5461 Å wavelength is 0.100 ± 0.002 minutes of arc per Oersted cm.

(b) The Solenoid

Despite having a low birefringent core, the solenoid is designed as a low power coil with a total resistance of approximately 1 ohm. The design parameters of several Faraday solenoids were studied, in particular the coil built by Gillham (1956) and, from the limited specifications available, a commercial coil marketed by Messrs. Bellingham and Stanley. The material used for the former is PTFE and the water tight sides are made of perspex. The coil is wound using 18swg enamelled copper wire. /

wire. The number of turns per layer was calculated as 82, and the nearest whole number of layers to give a resistance of about 1 ohm was determined to be 9. The coil was wound using an Avo Coil Winder, the exact number of turns being counted as 735. The fewer number of turns than expected is due to the oiled silk used between the layers enabling each layer to be directly on top of the previous one. The actual modulator dimensions are shown in Figure 3.4 and illustrated in Plate 5. The measured values of the completed solenoid are resistance: 1.0385Ω;
inductance: 3.138 mH.

(c) Check on Specification

Welsky (1960) shows that with multilayer coils where the spacing between the turns is sufficiently small for the inductance to be determined only by the number of turns and the overall dimensions of the winding then the Nagaoka constant K_n is a function of the length ℓ, the mean radius of the coil r, and the depth of the winding t.

ie,

$$K_n = 1/\{1 + 0.9\ (\frac{r}{\ell}) + 0.32\ (\frac{t}{r}) + 0.84\ (\frac{t}{\ell})\} \quad \text{---- (3.2.2)}$$

This for the above coil yields a factor of 0.694. Hence the theoretical coil inductance is given by the measured inductance divided by the Nagaoka constant, which comes to 4.48 mH. Using the expression for the numbers of turns of the coil of cross sectional area A as $N = \sqrt{I\ell/\mu A}$ where $\mu = 4\pi \times 10^{-7}$ then the theoretical number of turns is found to be 737 (cf 735 in practice).

The /

The coil to core length must be such that there is a minimum of nonuniformity due to end effects. In Figure 3.4 we have a longitudinal cross-section of the solenoid with N turns occupying length L metres. Hence the field produced by each loop at a point P on the axis and the field due to the loops carrying a current I in section δx is given by:

$$\delta B = \frac{\mu_o I}{2} \left[\frac{R^2}{(R^2 + x^2)^{3/2}}\right] \frac{N}{\ell} \cdot \delta x \qquad \text{---- (3.2.3)}$$

From the figure it is seen that

$x = R \cot\theta$ hence $dx = -R \operatorname{cosec}^2\theta d\theta$ and

$R^2 + x^2 = R^2(1+\cot^2\theta) = R^2 \operatorname{cosec}^2\theta$

Therefore

$$\frac{R^2\, dx}{(R^2+x^2)^{3/2}} = \frac{R^2(-R \operatorname{cosec}^2\theta\, d\theta)}{R^3 \operatorname{cosec}^3\theta} = -\sin\theta\, d\theta$$

$$\therefore dB = \frac{\mu_o I N}{2\ell} (-\sin\theta\, d\theta) \qquad \text{---- (3.2.4)}$$

For a solenoid of finite length the limits of θ at point P are θ_1 and θ_2.

$$\therefore B = \int dB = \frac{\mu_o I N}{2\ell} \int - \sin\theta d\theta$$

$$= \frac{\mu_o I N}{2\ell} [\cos\theta_1 - \cos\theta_2]$$

$$= \frac{\mu_o I N}{2\ell} \left[\frac{L - x}{\sqrt{[(L-x)^2 + r^2]}} + \frac{x}{\sqrt{[x^2 + r^2]}}\right]$$

$$\text{---- (3.2.5)}$$

The glass core is positioned such that the centre is at P', the centre of the solenoid, and one end is at P.

At /

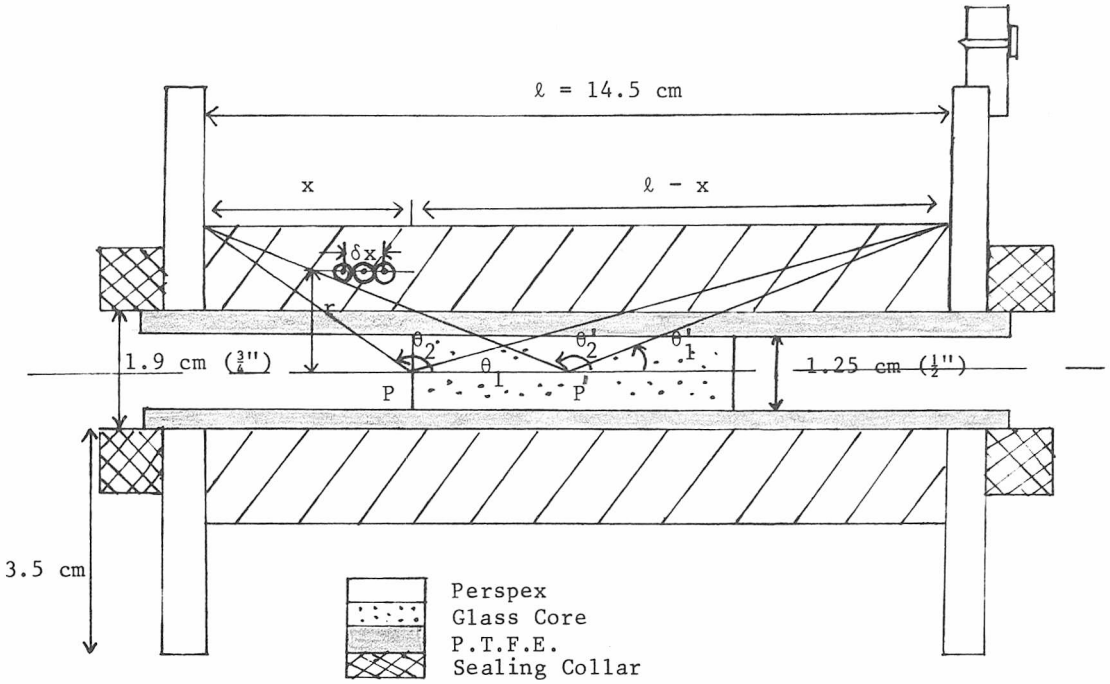

Figure 3.4 Longitudial cross-section of the Faraday Modulator.

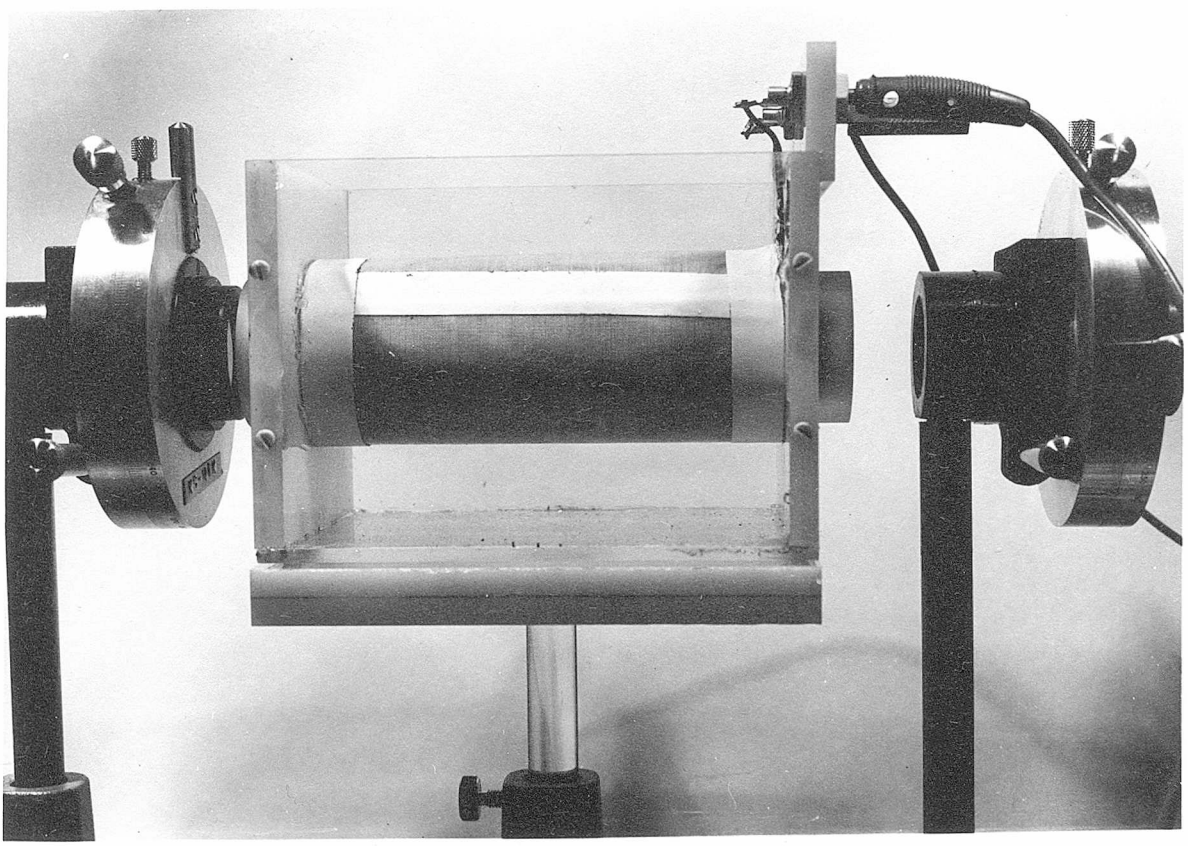

Plate 5 The Faraday Modulator.

At position P

$x = 3.25$ cm, $\ell - x = 8.25$ cm and $r = 1.55$ cm.

$$\frac{L - x}{\sqrt{[(L-x)^2 + r^2]}} + \frac{x}{\sqrt{[x^2 + r^2]}} = 0.983 + 0.903 = 1.886$$

At position P'

$x = 5.75$ cm

$$\cos\theta_1' - \cos\theta_2' = 2\left[\frac{x}{\sqrt{[x^2 + r^2]}}\right]$$

$$= 2 \times 0.967 = 1.934$$

It is therefore seen that for the length of solenoid chosen and for the particular core in use, the magnetic field at the edge of the core is less than 2.5% down on that at the core centre. The Verdet constant previously quoted as 0.100 minutes per Oersted centimetre which is equivalent to 0.126 minutes per ampere turn, means the production in the glass of a maximum rotation, with 1 amp. through the solenoid, of ± 1.543 degrees.

CHAPTER 4

ALIGNMENT PROCEDURE

The sensitivity of the ellipsometer is governed by:

1. the exactness with which the principle directions of the various optical components can be determined as being parallel or perpendicular to the plane of incidence,
2. the alignment of the optical components, and
3. how accurately the null position is found.

Correct alignment is critical for the accurate determination of the optical constants (n, k and d) of surfaces, although McCrackin et al (1963) indicate that for n and d measurement only, it is not quite as critical.

4.1.0 The Use of The Null Detection System

Since the divided circles used to mount the optical components were limited to the nearest 0.05 of a degree, the use of a phase sensitive detector giving a precision of 0.0001 of a degree, would have involved unnecessary expense. Instead the output from the photomultiplier tube is fed directly into an oscilloscope with a sensitivity of at least 10 $mV\,cm^{-1}$. The Faraday modulator is driven by a variable mains transformer giving a current of 1 ampere at mains frequency, designated the 'fundamental' frequency f_0. The corresponding sinusoidal axial magnetic field in the solenoid produces sinusoidal magneto-optical activity in the core material. The angle of rotation at 1 ampere has been shown in section 3.2.3c to be ±1.543 degrees. The oscillating beam emerging from the modulator strikes the analyzer at normal incidence. /

incidence. When the transmission axis of the analyzer is at right angles to the mean position of the plane of polarization the analyzer is in the null position. With no magnetic field in the Faraday modulator this corresponds to extinction, however because of the a.c. magnetic field in the solenoid, the azimuth of the plane of polarization of the incident light, ψ, relative to the transmission axes of the analyzer, will change sinusoidally. This results in a time varying intensity I(t) incident upon the photomultiplier.

If α is the angle between the transmission axes of the polarizer and analyzer, and Θ is the rotation in the direction of increasing α caused by the Faraday modulator then assuming there is no optically active material between the polarizer and the modulator, Williamson et al (1964) shows that the intensity of light I(t) is given by

$$I(t) = C \cos^2(\alpha+\Theta)$$

$$= (C/2)(1+\cos 2\alpha \cos 2\Theta - \sin 2\alpha \sin 2\Theta) \quad \text{---- (4.1.1)}$$

where C is some proportionality constant.

The Fourier-series expansion of I(t) in terms of the harmonics of f_o when $\Theta = \Theta_o \sin 2\pi f_o t$ yields

$$I(t) = (C/2)\{1 + \cos 2\alpha [(1 - \Theta_o^2 + \Theta_o^4/4) + (\Theta_o^2 - \Theta_o^4/3)\cos 4\pi f_o t + \ldots\ldots] - \sin 2\alpha [(2\Theta_o - \Theta_o^3 + \Theta_o^5/6)\sin 2\pi f_o t + (\Theta_o^3/3 - \Theta_o^5/12)\sin 6\pi f_o t + \ldots\ldots]\}$$

---- (4.1.2)

Since /

Since Θ_0 is small only the lower order terms of Θ_0 are considered.

When the analyzer is in the null position ($\alpha = \pi/2$), then I(t) contains essentially only the harmonic component of $2f_0$ and as the analyzer is moved from the null, the $2f_0$ component of I(t) diminishes and the f_0 component increases. The waveforms of I(t) are shown in Plate 6 for the exact null position and analyzer settings near the null position. In passing through the null the amplitude of the fundamental component passes through zero and undergoes a π phase change.

4.2.0 Setting the Optical System

Before measurements can be made with the ellipsometer, the instrument must be aligned so that the photocathode of the photomultiplier tube receives the maximum obtainable light flux, and the characteristic eigenvectors of the polarizer, analyzer and $\lambda/4$-plate must be established.

4.2.1 Determination of the Polarizer and Analyzer Transmission Directions

It is necessary to determine the divided circle scale reading for which the plane of vibration of the light transmitted by the polarizer or analyzer is parallel to the plane of incidence. Equation (2.1.22) indicates that at the polarizing angle of incidence the direction of the reflected linearly polarized electric eigenvector is normal to the plane of incidence. Hence a clean glass sample, in this case Schott BK7 glass which has a very thin natural surface (Vašíček, 1947), is positioned in the ellipsometer to reflect unpolarized monochromatic light at the polarizing angle.

ie, /

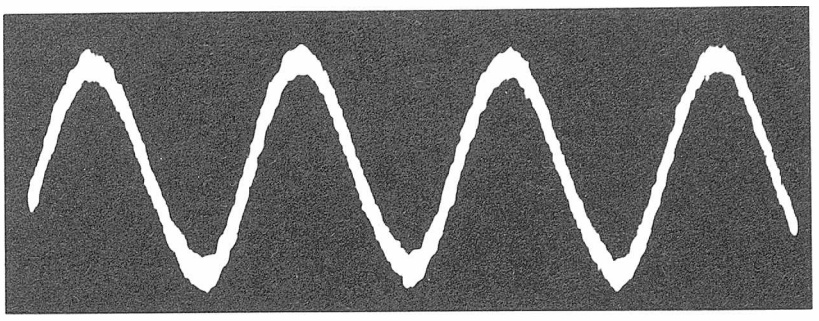

Null Position

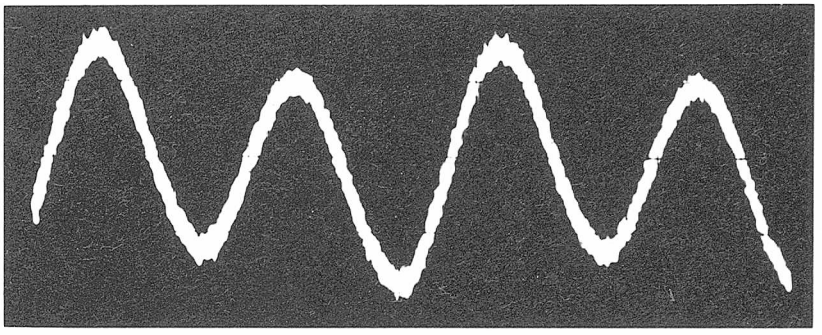

+ 0.05° of Arc from Null

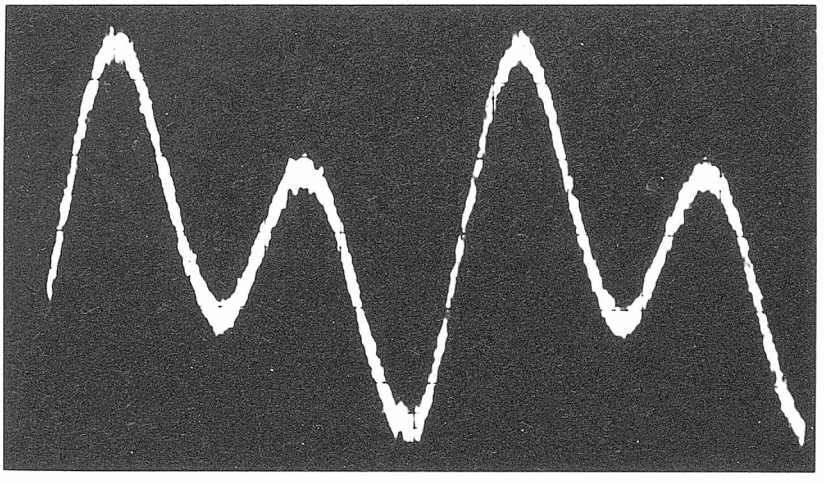

+ 0.10° of Arc from Null

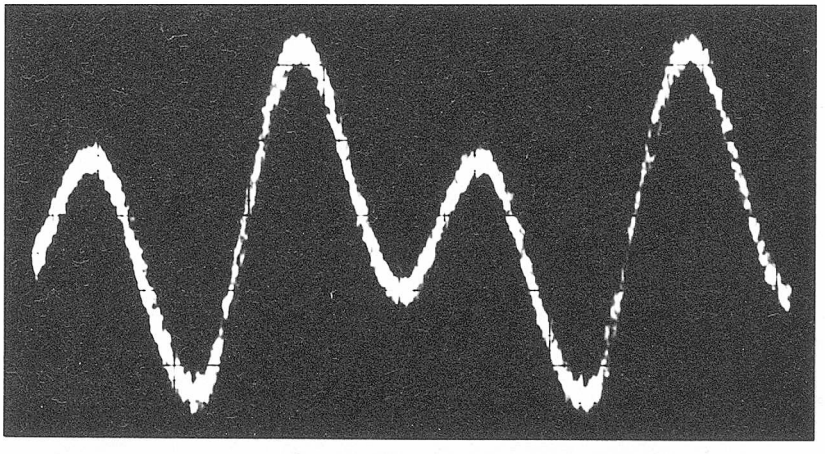

- 0.10° of Arc from Null

Plate 6 Photomultiplier Current I (t) for different Analyzer Settings near the Null Position.

ie, If n_2 is the refractive index of BK7 glass which for 5461Å is quoted as 1.51872 then

$$\phi_{Op} = \arctan n_2 = \arctan 1.51872$$
$$= 56^\circ\ 38'.$$

The polarizer or analyzer when placed in the emergent arm will therefore completely extinguish the light beam when its transmission direction is parallel to the plane of incidence. The two readings for which the null occurs for both the polarizer and analyzer are noted as future reference points.

4.2.2 Determination of the λ/4-Plate Fast and Slow Vibration Directions

It is also necessary to know the fast and slow vibration directions of the λ/4-plate with respect to the divided circle scale, and also which direction is which.

With the polarizer in the incident arm, the analyzer in the emergent arm and the ellipsometer in a linear configuration, the null position for the crossed polarizers is obtained. The λ/4-plate is then placed on the emergent arm between the crossed polarizers and the four readings which re-establish the null position, where the vibration directions are parallel to the polarizer and analyzer transmission directions, are noted.

Which pair of readings represents which vibration direction is determined by making use of a λ/4-plate of known slow (and hence fast) direction. Provided the unknown λ/4-plate is slightly away from a null setting then two fast or slow axes placed parallel will move the resultant further from the null, whereas /

whereas a fast axis parallel to a slow axis will in effect cancel the λ/4-plate retardation, resulting in the null position being restored. Hence the λ/4-plate to be calibrated is set with one vibration direction parallel to the plane of incidence so that the null position is observed accurately on the oscilloscope. The λ/4-plate is then moved approximately 3°, in either direction, away from this position. The known λ/4-plate is then placed in the light path on the incident arm, and rotated until the null position is once again established. This will occur in only one direction of the known λ/4-plate and indicates that the particular vibration direction is in fact the opposing one. That is, if the known λ/4-plate vibration direction is slow then the unknown direction is fast and vice versa. The pair of readings which corresponds to each vibration direction is hence found and noted.

4.2.3 Sample Alignment

It is desirable from the point of view of reproducibility and compatability of results, and also necessary for accurate angle of incidence setting, that a sample holder and alignment system be devised that is convenient, simple and precise. Plate 2 illustrates the sample holder and Plate 3 shows the alignment beam source and target at point X. The 0.1 mW helium-neon laser (used since it is a convenient source of coherent light) and target point X, are initially carefully set to be at the same height and equidistant from the transverse centre of the optical bench. Now a sample is placed in the holder, the latter is moved until the beam hits and covers the target, indicating that the sample is directly above the axis of rotation, lying in the same vertical plane and normal to the incident arm. The precision is varied by altering the path length. The distance used in practice is of the order of 1.75 metres.

4.2.4 /

4.2.4 Instrument Alignment and Experimental Technique

Measurements are best carried out in a darkened room, the collimator and telescope being initially set to produce and receive parallel light. A specimen for investigation is placed in the sample holder and aligned as described in section 4.2.3. The sample is then rotated to such an angle that the laser beam is reflected along the transverse centre of the incident arm. The optical components are moved, if need be, until their centres lie in the same horizontal plane and the laser beam passes unobstructed along the arm. The sample holder is then removed and the light source switched on to its maximum wattage so that the incident arm may be aligned using the light beam. Next the photomultiplier housing is removed from the end of the telescope and the incident arm shifted until the image of the lamp filament is in the centre of the field of view. If the photomultiplier housing is replaced, and the EHT supply and modulator current switched on, the instrument is now operational in the linear mode, enabling the polarizer and analyzer transmission settings to be checked. Slight variation in the settings are usually found due to loss of polarization, however this can be compensated for by altering the initial analyzer position by approximately 0.5°. A check is also made on the $\lambda/4$-plate vibration directions, although these should not change.

To measure the thickness and/or the refractive index of a film deposited on a substrate or the refractive index of a bare substrate, the sample holder is replaced in the turntable and the sample aligned, using the laser and target, to be normal to the incident arm. The turntable is then rotated to the desired angle of incidence (correct to the nearest minute of arc) and the emergent arm swung round to receive the reflected image. The /

The image is checked for position and if found to have deviated due to the nonuniformity of the table, is returned to the centre of the field of view by adjusting the telescope. The ellipsometer is now aligned and ready for use.

CHAPTER 5

DATA HANDLING

It is essential that the determination of the parameters of a specimen under investigation can be evaluated quickly and accurately from the measurements made by the ellipsometer. The three main methods of interpretation are graphical, computational and a mixture of both. Hence it is necessary to know the relationship between all the elliptic parameters and the measurements made, and how the refractive index and/or thickness can be found from this relationship.

5.1.0 Determination of γ and χ from Ellipsometric Measurements

The effect of the optical components of the ellipsometer upon the light beam is shown in Figure 3.1. The incident angle, ϕ_0, selected is generally 60° which is close to the polarizing angle for most substrates and in the area of highest sensitivity. However, King and Downs (1969) show that in the range 55° to 70° one might expect little variation in the results. The planes marked A_0, A_1 and A_2, correspond to the axes A_0A_0', A_1A_1', and A_2A_2' in Figure 2.4 and are the various positions of the analyzer measurements made in sequence. The position A_0 is the setting of the analyzer when its transmission axis is along A_0A_0'. With the $\lambda/4$-plate removed from the ellipsometer, the polarizer is turned so that its transmission axis is at an angle of 45° to the horizontal, as measured looking towards the source, and the analyzer rotated until the null position is found. This setting, A_1, is that at which the analyzer transmission direction lies along the axis A_1A_1'. The ellipse, resulting from reflection at the specimen lies in a quadrant which varies according to the size and sign /

sign of γ and ψ. This quadrant position is as predicted in Figure 2.5 page 23.

From Figure 2.4 it can be seen that

$$\chi - 90^\circ = A_1 - A_0 \qquad \text{---- (5.1.1)}$$

To measure the ellipticity γ, the $\lambda/4$-plate is inserted in the emergent arm at an angle of $(B+\chi)^\circ$ where B is the vernier scale reading when the slow axis of the $\lambda/4$-plate is horizontal. The insertion of the $\lambda/4$-plate causes a movement away from the null position as indicated on the oscilloscope. The analyzer has to be rotated until the null position is once again restored. This occurs for movement of the analyzer in one direction only which determines the sign of γ. In this position, A_2, the transmission axis of the analyzer is normal to the resultant vibration vector of the $\lambda/4$-plate.

Clearly, from Figure 2.4

$$\gamma = A_2 - A_1 \qquad \text{---- (5.1.2)}$$

If a set of films of known refractive index and thickness are measured using the ellipsometer then the corresponding values of χ and γ are obtained. Hence the simplest data handling method is to plot curves of χ versus γ for values of n_1 and d_1. From these curves the thickness and refractive index of unknown films can be interpolated using their measured values of χ and γ.

5.2.0 The Relationship Between γ, χ and ψ, Δ.

One computational-graphical data handling technique, initially used by Archer (1962), is the logical extension of the above, where curves of ψ versus Δ are plotted for various values of n_1 and d_1.

5.2.1 The Derivation of ψ in Terms of χ and γ

The azimuth angle ψ, and the phase difference Δ are shown to be related to the measured characteristics of the ellipse χ and γ by the equations

$$\tan 2\chi = \tan 2\psi \cos\Delta \qquad \text{---- (2.3.16)}$$

and

$$\sin 2\gamma = \pm \sin 2\psi \sin\Delta \qquad \text{---- (2.3.19)}$$

Hence by eliminating Δ we get

$$1 = \cos^2\Delta + \sin^2\Delta = \tan^2 2\chi/\tan^2 2\psi + \sin^2 2\gamma/\sin^2 2\psi \qquad \text{---- (5.2.1)}$$

$$\therefore \tan^2 2\chi(\cot^2 2\psi) + \sin^2 2\gamma \operatorname{cosec}^2 2\psi = 1$$

ie

$$\tan^2 2\psi(\operatorname{cosec}^2 2\psi - 1) + \sin^2 2\gamma \operatorname{cosec}^2 2\psi = 1$$

$$\therefore \operatorname{cosec}^2 2\psi[\tan^2 2\chi + \sin^2 2\gamma] = 1 + \tan^2 2\chi$$

$$\operatorname{cosec}^2 2\psi = \frac{1 + \tan^2 2\chi}{\tan^2 2\chi + \sin^2 2\gamma} = \frac{\sec^2 2\chi}{\tan^2 2\chi + \sin^2 2\gamma}$$

$$1 + \cot^2 2\psi = \frac{\sec^2 2\chi}{\tan^2 2\chi + \sin^2 2\gamma}$$

$$\therefore \quad \cot^2 2\psi = \frac{\sec^2 2\chi - \tan^2 2\chi - \sin^2 2\gamma}{\tan^2 2\chi + \sin^2 2\gamma}$$

But

$$\sec^2 2\chi = 1 + \tan^2 2\chi$$

$$\therefore \quad \cot^2 2\psi = \frac{\cos^2 2\gamma}{\tan^2 2\chi + \sin^2 2\gamma}$$

$$\therefore \quad \tan^2 2\psi = \frac{\tan^2 2\chi + \sin^2 2\gamma}{\cos^2 2\gamma}$$

$$\therefore \psi = \tfrac{1}{2}\arctan\left[\left(\frac{\tan^2 2\chi + \sin^2 2\gamma}{\cos^2 2\gamma}\right)^{\frac{1}{2}}\right] \qquad \text{---- (5.2.2)}$$

5.2.2 The Derivation of Δ in Terms of χ and γ

Eliminating ψ from equations (2.3.16) and (2.3.19) we get:

$$\frac{\tan 2\chi}{\sin 2\gamma} = \pm \frac{\tan 2\psi \cos\Delta}{\sin 2\psi \sin\Delta}$$

$$= \pm \frac{1}{\cos 2\psi} \cdot \frac{1}{\tan\Delta}$$

$$\therefore \tan\Delta = \pm \frac{\sin 2\gamma \cos 2\chi}{\cos 2\psi \sin 2\chi}$$

$$\therefore \Delta = \pm \arctan\left[\frac{\sin 2\gamma \cos 2\chi}{\cos 2\psi \sin 2\chi} \right] \quad \text{---- (5.2.3)}$$

But from equation (5.2.1),

$$\cos^2 2\psi \tan^2 2\chi + \sin^2 2\gamma = \sin^2 2\psi$$

ie,

$$\cos^2 2\psi \left(\frac{1 - \cos 2\chi}{\cos^2 2\chi}\right) + (1 - \cos^2 2\gamma) = 1 - \cos^2 2\psi$$

$$\cos^2 2\psi (1-\cos^2 2\chi) + \cos^2 2\chi (1-\cos^2 2\gamma) = \cos^2 2\chi (1-\cos^2 2\psi)$$

$$\therefore \cos^2 2\psi - \cos^2 2\psi \cos^2 2\chi + \cos^2 2\chi - \cos^2 2\chi \cos^2 2\gamma$$

$$= \cos^2 2\chi - \cos^2 2\chi \cos^2 2\psi$$

$$\therefore \cos 2\psi = \cos 2\chi \cos 2\gamma \quad \text{---- (5.2.4)}$$

Substituting equation (5.2.4) into equation (5.2.3) yields

$$\Delta = \pm \arctan \left[\frac{\sin 2\gamma \cos 2\chi}{\cos 2\gamma \cos 2\chi \sin 2\chi} \right]$$

$$= \pm \arctan \left[\frac{\tan 2\gamma}{\sin 2\chi} \right] \quad \text{---- (5.2.5)}$$

5.3.0 /

5.3.0 The Evaluation of Thickness and Refractive Index from Q

It is possible to obtain values of the thickness and refractive index of a film explicitly from Q and the basic equation of ellipsometry (equation (2.3.20)) once ψ and Δ are known.

ie,

$$\tan\psi \exp(i\Delta) = Q = R_p^+/R_s^+$$

$$= \frac{r_{01}^p + r_{12}^p \exp(-D)}{1 + r_{01}^p r_{12}^p \exp(-D)} \cdot \frac{1 + r_{01}^s r_{12}^s \exp(-D)}{r_{01}^s + r_{12}^s \exp(-D)}$$

$$= \frac{r_{01}^p + r_{12}^s \exp(-D) + r_{01}^p r_{01}^s r_{12}^s \exp(-D) + r_{12}^p r_{01}^s r_{12}^s [\exp(-D)]^2}{r_{01}^s + r_{01}^s r_{01}^p r_{12}^p \exp(-D) + r_{12}^s r_{01}^p r_{12}^p [\exp(-D)]^2 + r_{12}^s \exp(-D)}$$

ie,

$$\tan\psi \exp(i\Delta) [\, r_{01}^s + r_{01}^s r_{01}^p r_{12}^p \exp(-D) + r_{12}^s r_{01}^p r_{12}^p [\exp(-D)]^2 + r_{12}^s \exp(-D)]$$

$$= r_{01}^p + r_{12}^p \exp(-D) + r_{01}^p r_{01}^s r_{12}^s \exp(-D) + r_{12}^p r_{01}^s r_{12}^s [\exp(-D)]^2$$

This may be written as a quadratic in exp(-D) namely

$$k_1[\exp(-D)]^2 + k_2 \exp(-D) + k_3 = 0 \qquad \text{---- (5.3.1)}$$

where $k_1 = Q.r_{12}^s r_{01}^p r_{12}^p - r_{12}^p r_{01}^s r_{12}^s$

$k_2 = Q(r_{01}^s r_{01}^p r_{12}^p + r_{12}^s) - r_{01}^p r_{01}^s r_{12}^s - r_{12}^p$

$k_3 = Q.r_{01}^s - r_{01}^p$

Equation (5.3.1) has two roots q and v which are complex.

ie $q = q_R + iq_I$ and $v = v_R + iv_I$

Hence for the first root q:-

$$q = \exp(-D_A) = \exp -(D_{AR} + iD_{AI})$$

$$= \exp(-D_{AR}) \cdot \exp(-iD_{AI})$$

$$= \exp(-D_{AR}) [\cos(D_{AI}) - i \sin(D_{AI})]$$

$$\therefore q_R = \exp(-D_{AR}) \cos D_{AI} \quad \text{---- (5.3.2)}$$

and

$$q_I = -\exp(-D_{AR}) \sin D_{AI} \quad \text{---- (5.3.3)}$$

Therefore, $D_{AI} = \arctan(-q_I/q_R)$ ---- (5.3.4)

Squaring equations (5.3.2) and (5.3.3) and adding, gives:-

$$1 = (q_R^2 + q_I^2)/\exp^2(D_{AR})$$

$$\therefore (\exp D_{AR})^2 = |q|^2$$

ie $\exp D_{AR} = |q|$

and $D_{AR} = \ln |q|$ ---- (5.3.5)

Similarly $v = \exp D_B$ yields

$$D_{BI} = \arctan(-v_I/v_R)$$

and

$$D_{BR} = \ln |v|$$

Rearranging /

Rearranging equation (2.2.6) enables the physical thickness d to be found

ie,

$$d = D\lambda/4\pi i\ n\ \cos\phi$$

in general.

Hence for root q

$$d = -iKD_{AR}/n + KD_{AI}/n$$

where

$$K = \lambda/4\pi\ \cos\phi$$

If n is real then

$$d = -i\ d_{AR} + d_{AI} \qquad \text{---- (5.3.6)}$$

If n is complex, ie,

$$N = n + ik$$

then

$$d = \frac{-iK(nD_{AR} + kD_{AI})}{n^2 + k^2} + \frac{K(nD_{AI} + kD_{AR})}{n^2 + k^2} \qquad \text{---- (5.3.7)}$$

Similarly for root v.

It has been shown that Q is a function of n, d and for an absorbing film k. The mathematics are so complex that their manipulation would be tedious, however computer program methods allow rapid solution once the program has been established. Two distinct methods are available, one using a matrix method of calculation (Hayfield and White,(1964)) which allows curves of Q to be drawn and hence is a computational-graphical data handling technique. The values of n, k and d are then found from these curves. The other solely computational method (McCrackin et al, (1963)), is used as the basis of a program to enable n and d to be calculated explicitly as outlined above.

5.4.0 The Evaluation of the Refractive Index of a Bare Substrate from Q

The complex refractive index of a reflecting bare substrate can be calculated from Q and hence from the measurements made with the ellipsometer. Equation (2.3.20) yields:-

$$Q = \tan\psi \exp(i\Delta)$$

$$= \frac{r_{02}^{p}}{r_{02}^{s}} \quad \text{for a bare substrate.}$$

$$= \frac{n_2 \cos\phi_0 - n_0 \cos\phi_2}{n_2 \cos\phi_0 + n_0 \cos\phi_2} \cdot \frac{n_0 \cos\phi_0 + n_2 \cos\phi_2}{n_0 \cos\phi_0 - n_2 \cos\phi_2}$$

$$= \frac{n_2 n_0 \cos^2\phi_0 + n_2^2 \cos\phi_0 \cos\phi_2 - n_0^2 \cos\phi_0 \cos\phi_2 - n_0 n_2 \cos^2\phi_2}{n_2 n_0 \cos^2\phi_0 - n_2^2 \cos\phi_0 \cos\phi_2 + n_0^2 \cos\phi_0 \cos\phi_2 - n_0 n_2 \cos^2\phi_2}$$

$$= \frac{n_2 n_0 (\cos^2\phi_0 - \cos^2\phi_2) + \cos\phi_0 \cos\phi_2 (n_2^2 - n_0^2)}{n_2 n_0 (\cos^2\phi_0 - \cos^2\phi_2) - \cos\phi_0 \cos\phi_2 (n_2^2 - n_0^2)}$$

But from Snell's Law, ie, equation (2.1.12)

$$n_0 \sin\phi_0 = n_2 \sin\phi_2$$

$$n_2^2 \sin^2\phi_2 = n_0^2 (1 - \cos^2\phi_0)$$

$$\cos^2\phi_0 = 1 - \frac{n_2^2}{n_0^2} \sin^2\phi_2 \qquad \text{---- (5.4.1)}$$

$$\cos^2\phi_0 - \cos^2\phi_2 = -\cos^2\phi_2 + 1 - \frac{n_2^2}{n_0^2} \sin^2\phi_2$$

$$= 1 - \frac{n_2^2}{n_0^2} \sin^2\phi_2 - (1 - \sin^2\phi_2)$$

$$= /$$

$$= \sin^2\phi_2\left(1 - \frac{n_2^2}{n_o^2}\right)$$

$$= \frac{n_o^2}{n_2^2}\left(1 - \frac{n_2^2}{n_o^2}\right)\sin^2\phi_o$$

$$= \frac{n_o^2 - n_2^2}{n_2^2}\sin^2\phi_o$$

Hence,

$$Q = \frac{\frac{n_o}{n_2}(n_o^2-n_2^2)\sin^2\phi_o + \cos\phi_o\cos\phi_2(n_2^2-n_o^2)}{\frac{n_o}{n_2}(n_o^2-n_2^2)\sin^2\phi_o - \cos\phi_o\cos\phi_2(n_2^2-n_o^2)}$$

$$= \frac{n_o \sin^2\phi_o - n_2 \cos\phi_o \cos\phi_2}{n_o \sin^2\phi_o + n_2 \cos\phi_o \cos\phi_2}$$

$$\therefore Q + 1 = \frac{n_o\sin^2\phi_o - n_2\cos\phi_o\cos\phi_2 + n_o\sin^2\phi_o + n_2\cos\phi_o\cos\phi_2}{n_o\sin^2\phi_o + n_2\cos\phi_o \cos\phi_2}$$

$$= \frac{2n_o \sin^2\phi_o}{n_o \sin^2\phi_o + n_2 \cos\phi_o \cos\phi_2}$$

$$n_2\cos\phi_o\cos\phi_2 = \frac{2n_o \sin^2\phi_o}{1 + Q} - n_o \sin^2\phi_o$$

$$= n_o \sin^2\phi_o \left[\frac{2}{1 + Q} - 1\right]$$

$$= n_o \sin^2\phi_o \frac{(1-Q)}{(1+Q)}$$

$$n_2 \cos\phi_2 = n_o \sin \phi_o \tan\phi_o \frac{(1-Q)}{(1+Q)}$$

But /

But,

$$\cos\phi_2 = \left[1 - \frac{n_0^2}{n_2^2}\sin^2\phi_0\right]^{\frac{1}{2}}$$

cf equation (5.4.1).

$$\therefore n_2^2\left[1 - \frac{n_0^2}{n_2^2}\sin^2\phi_0\right] = n_0^2\sin^2\phi_0\tan^2\phi_0\frac{(1-Q)^2}{(1+Q)^2}$$

$$\therefore n_2^2 - n_0^2\sin^2\phi_0 = n_0^2\sin^2\phi_0\tan^2\phi_0\frac{(1-Q)^2}{(1+Q)^2}$$

ie

$$n_2^2 = n_0^2\sin^2\phi_0 + n_0^2\sin^2\phi_0\tan^2\phi_0\frac{(1-Q)^2}{(1+Q)^2}$$

$$\therefore n_2 = n_0\sin\phi_0\left[1 + \left(\frac{1-Q}{1+Q}\right)^2\tan^2\phi_0\right]^{\frac{1}{2}} \quad \text{---- (5.4.2)}$$

5.5.0 The Computer Program

As indicated in sections 5.3.0 and 5.4.0 it is possible to compute explicit values of refractive index and thickness of thin films as well as the refractive index of a bare substrate. To this end a FORTRAN program was written for use on an Elliot 4100 computer. The skeleton flowchart is shown in Figure 5.1. The program can be divided into four main parts as indicated by the control variable M, (where $0 < M \leqslant 4$) and can accommodate N sets of results on any one run (where $0 < N \leqslant 50$).

The first part of the program, which is common to all computations, calculates values of χ, γ, ψ, Δ and Q for each set of A_0, A_1 and A_2 corresponding to particular values of n_1, d_1 and ϕ_0. Equations (5.2.2), (5.2.5) and (5.4.2) were derived for ease of computation however further simplification proved necessary.

The /

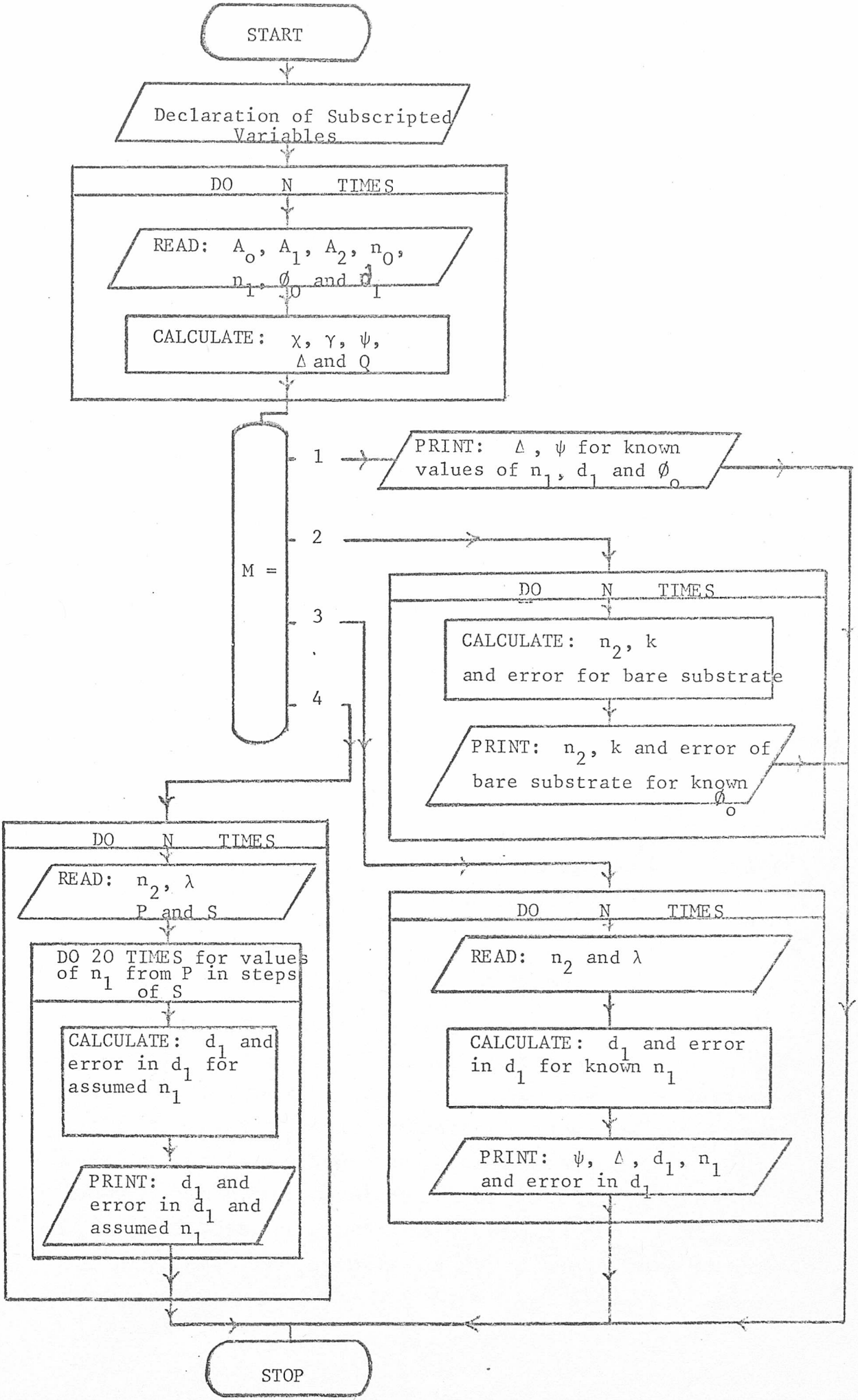

Figure 5.1 Skeleton Flowchart for Computer Program.

The next part of the program uses the generated value of Q in equation (5.4.2) to calculate the complex refractive index of the bare substrate. The real part becomes n_2 while the imaginary part becomes k. If the thin film under investigation is known to have k = 0, then the value computed for k is used as a measure of the experimental error. Only dielectric or weakly absorbing films are considered in this thesis.

The third section of the program uses the generated values of ψ and Δ, and the logic of section 5.3.0 to calculate values of the film thickness d_1 for known refractive index n_1. Since the physical thickness d_1 is real, the program scans for a minimum imaginary part in equation (5.3.6) and prints out the corresponding value of d_1, the small imaginary part being used to estimate the experimental error.

The final section of the program is essentially the same as part three, differing only in that a number of assumed values for the refractive index n_1 are taken and the corresponding values of d_1 then calculated. The correct pair of values is found when the error in d_1 is a minimum.

The actual program is reproduced in Appendix I and the key to functions and variables is given in Appendix II.

5.5.1 Verification of the Computer Program

The program was checked using results from a paper by Vašíček (December, 1947). In this paper he gives values of refractive index n_1, thickness d_1, incident angle ϕ_0, χ, γ and the corresponding ψ and Δ. His results for ϕ_0, χ and γ of a thin film of refractive index n_1 on a glass substrate of refractive index $n_2 = 1.5163$ (Schott BK7) were used as input data for the program. The outputs of d_1, ψ and Δ were in complete agreement /

agreement with Vašíček's results as is shown in Table 5.1. This validates both the mathematical approach and the program. The error in the thickness, δd, is also given in the output and can be seen to be less than ±0.02% which is to be expected and can be attributed to his computational technique. Using experimental results, the error in the thickness is a measure of the experimental error.

Table 5.1

Input data tabulated against results from Vašíček and compared to those obtained using the FORTRAN program

Input Data			Vašíček's Results			Calculated Results			
n_1	χ	γ	d(Å)	ψ	Δ	d(A)	ψ	Δ	δd(Å)
1.40	95.38°	0.73°	100.0	5.43°	7.70°	103.27	5.43°	7.77°	0.0009
	95.58°	1.40°	200.0	5.74°	14.18°	200.83	5.75°	14.18°	0.0030
	95.89°	2.06°	300.0	6.23°	19.38°	300.48	6.24°	19.43°	0.0005
	96.34°	2.66°	400.0	6.87°	22.97°	393.66	6.80°	23.21°	0.0662
1.39	97.07°	4.40°	500.0	8.30°	34.37°	500.56	8.30°	32.36°	0.0002
	97.84°	5.23°	600.0	9.39°	34.37°	600.53	9.39°	34.34°	0.0662
	98.88°	5.88°	700.0	10.59°	34.33°	699.65	10.60°	34.31°	0.0621
	100.19°	6.24°	800.0	11.88°	32.43°	799.69	11.88°	32.44°	0.0000

CHAPTER 6

RESULTS

The physics of thin films and surfaces is very extensive, offering numerous areas for the application of ellipsometry. A comparatively recent survey by Neal and Fane (1973) describes the application of the different types of ellipsometer. An appraisal of the technique and some specific examples of application are found in the Washington Symposium, 'Ellipsometry in the Measurement of Surfaces and Thin Films' (Passaglia, 1964), and Surface Science (1969). Only the application to thickness measurement and refractive index for a dielectric film is considered in this thesis.

6.1.0 Method of Measurement

The method followed in the use of the ellipsometer is as below:

1. Determine the transmission directions of the polarizer and analyzer as outlined in section 4.2.1 and establish the vibration directions of the $\lambda/4$-plate as in section 4.2.2.
2. Align the instrument as in section 4.2.4 with the analyzer transmission direction in the horizontal position, A_o, and the polarizer normal to the plane of incidence.
3. Place a sample in the holder and align as in section 4.2.3.
4. The angle of incidence, ϕ_o, is now set using the turntable vernier to note the angle ($\phi_o = 60^\circ$ in this case).
5. /

5. The polarizer is turned so that, looking towards the source, the transmission direction is at an angle of 45° to the plane of incidence.

6. The λ/4-plate is removed and the detection system and light source switched on.

7. Now the analyzer is rotated until the null position is reached. This analyzer position A_1 is then read and noted.

8. From equation (5.1.1) the angle χ is hence found and the λ/4-plate set to an angle of $(B+\chi)°$, where B is the vernier scale reading when the slow axis of the λ/4-plate is parallel to the plane of incidence.

9. The λ/4-plate is inserted into the emergent arm and the analyzer rotated until the null position is restored. This analyzer position is read as A_2 and hence γ can now be calculated.

10. The readings A_0, A_1, and A_2, as well as the appropriate angle of incidence, wavelength and known or assumed values of n_1 and n_2 are fed into the computer. Since the immersion medium is air, a value of 1 is taken for n_0.

11. Finally the turntable is rotated back normal to the incident arm, and the alignment of the sample checked.

6.2.0 Evaluation of Errors and Accuracy

Instrumental errors, both random and systematic, occur in the use of the ellipsometer and these are carried over to the calculated film parameters.

In the optical system, multiple reflections produce beams of decreasing intensity and differing polarization states which influence the three analyzer readings. /

readings. For this reason the $\lambda/4$-plate used is not mounted between glass plates and the glass core of the Faraday modulator has antireflection coatings on either end. The residual stress birefringence of the core is almost zero as is that of the polarizer and analyzer, however some birefringence will be present in the $\lambda/4$-plate due to mounting in the divided circle.

The sensitivity of the detection system undoubtedly limits the accuracy of the instrument, especially when there is low light flux after reflection on the sample surface. Since the final determination of the null position is subjective, increasing the sensitivity of the oscilloscope has only a minimal effect. The voltage to the photomultiplier dynode chain can also be increased. This does increase the signal to noise ratio of the f_o component (see section 4.1.0) at either side of the null position, but as it is a minimum in this component that is required, and the $2f_o$ component is increasingly swamped by noise with increasing voltage, the setting of 750 volts is found to be the optimum.

The above random errors linked with the systematic errors arising from uncertainties in the initial alignment and the determination of the vibration directions of the optical components, makes the assessment of errors somewhat obscure. The accuracy of setting the angle of incidence is also important. However, for the present turntable this should only be of the order of 0.03° resulting in an undetectable change in the analyzer readings.

Some indication as to the order of accuracy in obtaining the χ and γ values, and where the largest errors might be expected, can be gauged by considering actual values.

The /

The analyzer setting A_0 has a value

$$A_0 = 206.20^\circ \pm 0.05^\circ$$

206.20° is the arbitrary angle where the transmission direction of the analyzer is parallel to the angle of incidence. One can read A_1 as some value $\mathbb{O} \pm 0.05^\circ$.

As mentioned above the estimation of the null position is subjective, however, it is observed that movement of the analyzer by 0.05° causes a noticeable change away from the null.

Hence $A_1 = \mathbb{O} \pm 0.10^\circ$

From equation (5.1.1) it is seen that

$$\chi - 90^\circ = A_1 - A_0 = \omega \pm 0.15^\circ$$

The setting of the $\lambda/4$-plate will effect the reading of A_2, as will the fact that for 5461Å there is an error of ±0.5Å in the plate, but these should be minimal.

Finally the analyzer setting A_2 has a value

$$A_2 = \Theta \pm 0.10^\circ$$

From equation (5.1.2)

$$\begin{aligned} \gamma &= A_2 - A_1 \\ &= \Theta \pm 0.10^\circ - \mathbb{O} \pm 0.10^\circ \\ &= \nabla \pm 0.20^\circ \end{aligned}$$

In general values of χ tend to be large, (80°) depending on the polarizer setting, whereas values of γ are small (2°) and can be less than one. Hence it is seen that while values of χ will for the most part result in errors <1%, errors in γ can be exceedingly high for this particular ellipsometer.

6.3.0 Actual Results Taken Using the Ellipsometer

6.3.1 The Samples

It was fortunate that a commercial enterprise depositing thin films for both optical and electronic applications was interested in the relatively cheap, yet accurate method of determining the thickness and refractive index of certain dielectric films that this ellipsometer offers. Also of future interest to them was a check on the refractive index of bare substrates before deposition.

Messrs OCLI Optical Coatings Ltd., a subsiduary of Optical Coating Laboratory Inc., Santa Rosa, California, USA at present do not batch check their substrates before deposition and use reflection spectrophotometry to check the thickness. These reflection scans, carried out on a Beckmann DK2 Spectrophotometer, are at best 3% accurate, but do not yield information about the refractive index.

The provision of several bare substrates of glass with a range of refractive index from approximately 1.5 to 1.7 and also a series of magnesium fluoride (MgF_2) films of thickness ranging from 1,000 to 9,000 Angströms from OCLI, is gratefully acknowledged.

The corresponding reflection scans for the MgF_2 films are given in Appendix 3, while Table 6.1 shows how the thickness values for these films can be determined from the various reflection scans.

6.3.2 The Measurement of the Refractive Index of Bare Substrates Using the Ellipsometer

An indication of the accuracy obtainable using the ellipsometer is best found when the measured parameter is /

is known absolutely. Messrs Schott, the suppliers of the bare substrates to OCLI, quote the refractive index of their glass substrates correct to five significant figures, whereas the thickness of the MgF_2 films is known only to a 3% accuracy.

The substrates used, and their quoted refractive index are BK7 (n = 1.51872), SK16 (n = 1.62286), and LAK25 (n = 1.69401).

Two samples of each refractive index were measured, one with a ground back surface, and one with a polished back surface. The measured values for the refractive index of these bare substrates, n_2, were calculated using the program described in section 5.5.0 with M = 2. The output is given in Table 6.2 for the six samples, before and after cleaning. Since it is not known whether the quoted values of refractive index are for ground or polished rear surfaces, or whether the glass is freshly cleaned, an overall average was therefore used. The order of accuracy was found to be better than 0.5%.

6.3.3 Measurement of Film Thickness Using the Ellipsometer

Usually the film thickness will be approximately known from perhaps a crystal deposition monitor, and, the ellipsometer used for precise measurement. From equation (2.2.6) it can be seen that values of χ and γ repeat cyclically in 2π increments of D. Hence for each cycle d changes in general by

$$d = \lambda/2n \cos\phi \qquad \text{---- (6.3.1)}$$

The series of MgF_2 films were deposited on BK7 glass substrates by OCLI, in sets of three, each set being on /

Table 6.1

The determination of the MgF_2 Film Thickness from the reflection scans in Appendix 3

Nominal Value (Å)	1000	2000	3000	4000	5000	6000	7000	8000	9000
Reflection Scan readings (nm) where $nd = \frac{m\lambda}{4}$ (m is the order and is shown in brackets, while n is taken as 1.38)	546(1)	534(2)	540(3)	1110(2)	542(5)	1075(3)	956 (4)	620 (7)	605 (8)
			394(4)	740(3)	452(6)	808(4)	765 (5)	542 (8)	540 (9)
				556(4)	389(7)	650(5)	642 (6)	484 (9)	488(10)
				454(5)		548(6)	549 (7)	436(10)	444(11)
				380(6)		472(7)	482 (8)	397(11)	408(12)
						414(8)	434 (9)		
						368(9)	391(10)		
Corresponding Values of d (Å)	989.31	1934.78	2934.78	4021.74	4909.42	5842.39	6927.54	7862.32	8768.12
			2855.07	4021.74	4913.04	5855.07	6929.35	7855.07	8804.35
				4028.99	4932.97	5887.68	6978.26	7891.30	8840.58
				4112.32		5956.52	6961.96	7898.55	8847.83
				4130.43		5985.51	6985.51	7911.23	8869.57
						6000.00	7076.09		
						6000.00	7083.34		
Average Reflectance Measurement of d (Å)	989.31	1934.78	2894.45	4063.04	4918.48	5932.45	6991.72	7883.69	8826.09

Table 6.2

The measured refractive index n_2 of bare substrates compared to the quoted values

Glass (Quoted n*)	Back Surface Ground (G) or Polished (P)	n_2 (Before Cleaning)		n_2 (After Cleaning)		Overall Average	Accuracy (%)
BK7 (1.51872)	1. G 2. P	1.5260 1.5078	1.5169	1.5296 1.5150	1.5223	1.5196	0.06
LAK25 (1.69401)	1. G 2. P	1.7114 1.7030	1.7072	1.7014 1.6892	1.6953	1.7013	0.43
SK16 (1.62286)	1. G 2. P	1.6326 1.6246	1.6286	1.6294 1.6104	1.6199	1.6243	0.09

* NB It is not known if this is for ground or polished glass or whether it is for freshly cleaned glass.

on one substrate. The incident light beam was therefore collimated so as to strike only one thickness at a time. Unfortunately, by the time the ellipsometer was operational the films were several months old, but it was assumed that, if anything, only the refractive index would have changed. This will be discussed later. Meanwhile the reflectance measurements shown in Table 6.1 were taken as the actual film thickness to within 3%. The value used for the refractive index of MgF_2 in these measurements was that generally used by OCLI and is 1.38.

In Table 6.3 the computer program output for M = 3 gives the ellipsometer measurements for the MgF_2 films compared to the reflectance measurements. Four independent measurements of each thickness were taken, the consistency being in general better than 3%. It can be pointed out here, although it is valid for measurements of refractive index as well, that the generated error value as described in section 5.5.0 is an estimate of how any experimental error in the measurement of χ and γ effects the thickness measurement. The relationship between these parameters has been shown to be complex, and can result in slightly different values of χ and γ producing the same computed thickness but with a different error component.

The accuracy of the ellipsometer measurements, using the reflectance measurements as standard, varies widely, with the majority being less than 3%, but with the 2,000, 4,000 and 7,000 Angström thicknesses showing rather high values.

6.3.4 The Consistency of χ and γ

In section 6.2.0 it was stated that errors in the measurement of γ could be high, a factor which might explain /

Table 6.3

The ellipsometer thickness measurements compared to the reflectance measurement of the MgF_2 films

OCLI Thickness		ELLIPSOMETER THICKNESS			
Nominal (Å)	Reflectance Measurement (Å) ± 3%	Measured d(Å)	Average d(Å)	Consistency (%)	Accuracy (%)
1000	989.31 ± 29.68	990.15 ± 0.87 989.48 ± 1.09 967.00 ± 15.00 985.07 ± 1.80	982.93	1.62	0.64
2000	1934.78 ± 58.04	2142.29 ± 10.02 2190.13 ± 3.00 2199.39 ± 2.94 2130.93 ± 0.87	2165.69	1.61	11.94
3000	2894.45 ± 86.83	2961.87 ± 5.62 2911.22 ± 7.74 2786.19 ± 53.68 2835.10 ± 25.55	2873.60	3.04	0.72
4000	4063.04 ± 121.89	4424.41 ± 9.84 4382.63 ± 7.35 4469.17 ± 10.84 4496.18 ± 12.31	4443.10	1.36	9.35

Table 6.3 Cont'd

OCLI Thickness		ELLIPSOMETER THICKNESS			
Nominal (A)	Reflectance Measurement (A) ± 3%	Measured d(A)	Average d(A)	Consistency (%)	Accuracy (%)
5000	4918.48 ± 147.55	5077.01 ± 4.46 5110.03 ± 9.28 5122.88 ± 13.61 5078.80 ± 0.01	5097.18	0.50	3.63
6000	5932.45 ± 177.97	5944.60 ± 18.67 5908.08 ± 21.78 5775.13 ± 56.99 5889.22 ± 48.04	5879.26	1.77	0.90
7000	6991.72 ± 209.75	7430.07 ± 0.28 7303.16 ± 4.14 7292.24 ± 3.67 7283.71 ± 4.33	7327.29	0.59	4.80
8000	7883.69 ± 236.51	8044.36 ± 7.92 8101.17 ± 46.34 7984.56 ± 50.55 8012.01 ± 55.57	8035.53	0.63	1.93
9000	8826.09 ± 264.78	8818.69 ± 85.06 8819.15 ± 44.73 8817.43 ± 57.19 8862.73 ± 37.21	8829.50	0.37	0.04

explain the variation in the accuracy of the ellipsometer thickness measurements. The corresponding χ and γ values for the four ellipsometer thickness readings from Table 6.3 are given in Table 6.4.

It is seen that with only one exception the consistency of the χ values is better than 1% whereas the consistency of the γ values is as high as 35% with one value as high as 87.50%. By excluding the pair of χ, γ values with an anomolous γ value, the consistency of the γ values was improved greatly, without affecting the consistency of the χ values adversely. Only for the 5,000 Angström thickness was this not done since the obvious inconsistency questioned the ability to select on the above criterion. Instead the last pair of γ and χ values were used since they yielded the lowest error value. The new average χ and γ values were then used to calculate an adjusted value for the thickness of the MgF_2 films. These are shown in Table 6.5 and compare favourably with the average thickness values of Table 6.3. It is interesting to note:-

1. that no great improvement in accuracy was achieved by the improvement in the consistency of γ.
2. the four anomolous high percentage accuracy values have negative values of γ (ie, right handed).

This latter point is difficult to explain, but since care was taken to obtain the null position by moving the analyzer divided circle in the same direction, an answer might be that this could result in an incorrect value of A_2 for a right handed ellipse, if a backlash error was involved.

6.3.5 /

Table 6.4

Examination of the consistency
of the χ and γ values

d (Nom) Å	1000		2000		3000		4000		5000	
Degrees	χ	γ	χ	γ	χ	γ	χ	γ	χ	γ
	77.20	3.55	82.30	-2.15	82.90	3.00	80.75	-3.00	83.60*	-0.05*
	78.30*	2.55*	83.00	-2.35	83.15	2.65	80.45*	-3.25*	84.55*	0.25*
	77.40	3.40	83.05	-2.30	83.10*	1.50*	81.05	-2.85	84.45*	0.30*
	77.25	3.50	83.00*	-3.00*	83.20	1.95	81.20	-2.70	84.70	-0.05
Average	77.54	3.25	82.84	-2.45	83.09	2.28	80.86	-2.95	84.33	0.17
Consistency (%)	0.98	21.54	0.65	22.45	0.23	34.21	0.51	10.17	0.87	87.50
Average Excluding (*) Values	77.28	3.48	82.58	-2.27	83.08	2.53	81.00	-2.85	84.70	-0.05
Consistency Excluding (*) Values	0.16	2.30	0.34	5.29	0.22	22.92	0.31	5.26	-----	-----

Table 6.4 Cont'd

d (Nom) Å	6000		7000		8000		9000	
Degrees	X	Y	X	Y	X	Y	X	Y
	79.20	2.95	84.15*	-1.60*	83.85*	2.90*	79.00	0.35
	79.50	2.95	84.00	-2.10	82.50	2.10	78.35	0.50
	80.50*	2.40*	83.00	-2.20	82.55	2.00	78.60	0.45
	79.80	2.35	82.90	-2.20	82.35	2.05	78.15*	0.25*
Average	79.75	2.66	83.51	-2.03	82.81	2.26	78.53	0.39
Consistency (%)	0.94	11.65	0.77	21.00	1.26	28.32	0.60	35.90
Average Excluding (*) Values	79.50	2.75	83.30	-2.17	82.47	2.05	78.65	0.43
Consistency Excluding (*) Values	0.38	14.55	0.84	1.38	0.15	2.44	0.45	18.60

Table 6.5

The adjusted thickness values with their corresponding χ, γ, ψ and Δ values as well as the accuracy compared to the reflectance scan thickness in Table 6.1

Adjusted Thickness d(Å)	χ(deg)	γ(deg)	ψ(deg)	Δ(deg)	Accuracy (%)
985.03 ± 1.36	77.28	3.48	13.10	15.93	0.43
2138.80 ± 8.04	82.58	-2.27	7.94	343.19	10.54
2905.63 ± 11.50	83.08	2.53	7.36	20.31	0.39
4463.30 ± 11.07	81.00	-2.85	9.43	342.10	9.85
5078.80 ± 0.01	84.70	-0.05	5.30	359.46	3.26
5915.17 ± 27.42	79.50	2.75	10.84	15.04	0.29
7318.79 ± 2.13	83.30	-2.17	7.04	341.87	4.69
7999.74 ± 50.68	82.47	2.05	7.80	15.42	1.77
8818.91 ± 60.12	78.65	18.60	11.36	2.23	0.08

6.3.5 The Measurement of Film Refractive Index Using The Ellipsometer

It was shown in section 6.3.2 that the measurement of the refractive index of a bare substrate could be determined by better than 0.5%. Since the thickness measurements using the ellipsometer were all of MgF_2 films it is reasonable to assume that the values of χ and γ from Table 6.5 would yield the same value for the refractive index and that this value would be accurate. The computer program was therefore run with M = 4 and the output value for the refractive index with the minimum error in the thickness (see section 5.5.0) found as given in Table 6.6. Also given in the table is the reflectance scan thickness adjusted to correspond with the computed refractive index.

Each set of data resulted in a minimum error value at the shown refractive index, except the set for 5,000 Angströms. The value indicated for this thickness was <1.35 however, since there was doubt about the χ and γ values as indicated above, the result was not included.

The average value for the refractive index of MgF_2 was found to be 1.428 with the consistency being better than 3%. This value for the refractive index of MgF_2 is somewhat higher than that used to compute the thickness in section 6.3.3 however the age of the films must be considered. Heavens and Smith (1957) give the refractive index for an aged MgF_2 film as 1.401 ± 0.002 and Abelès (1950) explains his value of 1.400 ± 0.002 from density considerations showing that the deposited film of MgF_2 contains some voids.

6.4.0 /

Table 6.6

The refractive index and thickness of the MgF_2 films using the χ and γ values from Table 6.5

Nominal d(Å)	1000	2000	3000	4000	5000	6000	7000	8000	9000
Computed Refractive Index (correct to nearest 0.005)	1.390	1.445	1.430	1.425	----	1.415	1.445	1.450	1.425
Corresponding Thickness d(Å)	991.62	1698.76	2959.69	4103.20	----	5872.78	6710.53	7934.68	8554.77
Adjusted Reflectance Thickness (Å)	982.19	1847.75	2793.25	3934.73	----	5785.72	6677.21	7503.10	8547.37
Accuracy of Adjusted Reflectance Thickness Measurement (%)	0.96	8.77	5.96	4.28	----	1.51	0.50	5.75	0.87

Average Refractive Index	1.428	Consistency (%)	2.66

6.4.0 Discussion of Results

The refractive index and thickness determination are inter-related and therefore the results will be considered together.

In section 6.3.2 it was indicated that the refractive index of a bare substrate could be measured to within an accuracy of 0.5%. Since this accuracy was found by comparing the measured average refractive index with an 'absolute' value, this should indicate precisely the order of accuracy expected using the ellipsometer to measure refractive index. However, when the refractive index of the MgF_2 films were calculated the consistency was no better than 2.66% with an average refractive index value of 1.428.

This value for the refractive index of MgF_2 of 1.428 is probably about 1-2% high, even for an 'aged' film, and is considerably higher than the 1.38 used in the thickness estimation. This might explain the variation in accuracy of the thickness measurement.

Table 6.7 compares the ellipsometer measured thickness and generated error value, with the thickness value obtained from the reflectance scans for a refractive index of 1.428. It is seen that, with the reflectance scan as reference, the accuracy is, on average, 3.2%, with a higher consistency of accuracy than shown in Tables 6.3 and 6.5. The reflectance scan thickness for n = 1.428 can however, only be taken as ±5% correct. The value of the reflectance scan thickness for n = 1.400 was therefore calculated as having an accuracy of ±3%. This value was then used to compare the ellipsometer value, giving a marked improvement in the accuracy.

The /

Table 6.7

The thickness of the MgF_2 films comparing the ellipsometer value with that obtained from the reflectance scans, using the average value for n of 1.428 and the correct value of 1.400

Nominal d(Å)	1000	2000	3000	4000	5000	6000	7000	8000	9000
Computed Thickness for n = 1.428 (Å)	1001.34 ± 22.94	1820.71 ± 1.22	2953.79 0.70	4083.96 0.08	4935.95 ± 0.01	5841.11 ± 2.00	6882.17 ± 0.516	7935.51 ± 13.24	8534.05 ± 0.58
Reflectance Thickness for n = 1.428 (Å) ±5%	956.06 ±47.80	1869.75 ± 93.49	2797.16 ±139.86	3926.47 ±196.32	4753.15 ±237.66	5733.04 ±286.65	6756.70 ±337.84	7618.69 ±380.90	8529.41 ±426.47
Accuracy n = 1.428 (%)	4.74	2.62	5.60	4.01	3.85	1.89	1.86	4.16	0.05
Reflectance Thickness for n = 1.400 (Å) ±3%	975.18 ±29.26	1907.13 ± 57.21	2853.10 ± 85.59	4004.99 ±120.15	4848.22 ±145.45	5847.70 ±175.43	6891.84 ±206.76	7771.07 ±233.13	8700.00 ±261.00
Accuracy n = 1.400 (%)	2.68	4.53	3.53	1.97	1.81	0.11	0.14	2.12	1.91

The final discrepancy could be accounted for by the fact that, so far, the assumption hss been made that the MgF_2 films were isotropic and homogeneous. King and Downs (1969) on comparing their ellipsometric measurements of MgF_2 with Talystep measurement, suggest that, to account for the differences they found, it would appear necessary to consider the possibility of anisotropy, inhomogeneity and also slight absorption in the films.

CHAPTER 7

CONCLUSION

Before commencing the construction of the ellipsometer it was necessary to search the literature. From this it became evident that the mathematics involved were, for the most part, not developed, as well as being scattered through several papers and text-books. Chapter 2 is therefore an attempt to present one particular coherent mathematical approach.

It was at the same time appreciated that some method of handling the ellipsometer results was required. This to some extent dictated the mathematical approach since it had to be in a form suitable for computer programming. The polarization state of a monochromatic linearly-polarized wave after reflection from a film is shown to be dependent on many factors including: the polarization state of the incident light, the refractive index of the film and substrate, the film thickness, the angle of incidence and the wavelength. In Chapter 5 the relationship of these parameters is related to the ellipsometer measurements, giving various data handling methods and the logic for the FORTRAN program listed in Appendix I.

The ellipsometer construction, described in Chapter 3, is for the particular configuration that the mathematics describe. The arrangement used is that where the $\lambda/4$-plate follows the sample and where the polarizer azimuth is fixed at 45° with the compensator and analyzer azimuths being varied to obtain the null position. Cost played a major role in the selection of the components. Despite this the optical components are of high quality, and with more accurate divided circles or goniometers combined with a phase sensitive detector, the ellipsometer with the same optical components would become a /

a very precise and sensitive research tool. At low light flux levels a minor improvement would be to use a photo-multiplier with a better spectral response compared to that used, with the tube cooled to reduce noise problems. The design and construction of the Faraday modulator was necessitated not only by cost, but also by the availability of a cell to match the low power requirement. A list of suppliers is given in Appendix IV for the ellipsometer components.

Alignment is described in some detail in Chapter 4 because this can lead to errors which, when combined with random and other systematic errors, affect the accuracy of measurement. Holmes and Feucht (1967) show that for the ellipsometer configuration used in this thesis there are two distinct settings for which compensation occurs. The errors are consequently reduced by taking sets of results at these two compensation-extinction positions, provided the polarization state of the reflected wave is not changing with time, as in the case of a fast growing film. For the ellipsometer configuration where the $\lambda/4$-plate azimuth is fixed and the polarizer and analyzer rotated to find the null, McCrackin et al (1963) show, using Poincaré sphere representation, that there are 16 possible compensator settings in all, 4 in each zone. Hence by averaging results in either zones 1 and 3, or zones 2 and 4, the errors are again minimised.

Although the project was to construct an ellipsometer it was felt to be only valid to test the finished instrument. Three methods were used. One was to take results from a paper by Vašíček (December, 1947), which essentially checked the mathematical approach and the associated program. The second test was to measure the refractive index of bare substrates using the ellipsometer and the program. These substrates were supplied by Messrs OCLI, Optical Coatings Ltd., and had a refractive index known to 10 parts in 10^6. The measured /

measured results were all within 0.5%. Hence the first two checks show that the mathematical method and the ellipsometer are functioning as predicted.

The final test was to use a series of films supplied again by OCLI. These were in sets of three on one substrate. The refractive index was not known by OCLI very accurately, and the thickness was measured by reflectance spectrophotometry with a claimed accuracy of ±3%. The film material however, was MgF_2, so that the refractive index was known to be in the region of 1.4.

The data obtained from these films show that proper care must be taken in the interpretation of the results as outlined in Chapter 6. Assuming the refractive index of MgF_2 is 1.400 then the measured value is ±2%. Using the reflectance scan measurements as standard, the thickness is correct to ±2% on average. This order of accuracy compares favourably with other workers using ellipsometry (King and Downs, 1969), despite the lower precision invoked by low cost.

REFERENCES

Abelès, F., C.R. Acad.Sci. (Paris), 228, 553-5 (1949).

Abelès, F., J.Phys. et Radium, 11, 310-4 (1950).

Abelès, F., Progress in Optics, Vol.2, 249-87 (North-Holland Publishing Co., Amsterdam, (1963)).

Archer, R.J., J.Opt.Soc.Amer., 52, 970-77 (1962).

Behrndt, K.H., Physics of Thin Films Vol.3, 1-59, (G. Hass and R.E. Thun, Eds., Academic Press Inc., New York, 1966).

Bennett, H.E., and Bennett, J.M., Physics of Thin Films, Vol.4, 1-96, (G. Hass and R.E. Thun, Eds., Academic Press Inc., New York, 1966).

Bom, M., and Wolf, E., Principles of Optics, 4th Edition (Pergamon Press Ltd., London, 1970).

Coulson, C.A., Waves, 102-127 (Oliver and Boyd Ltd., Edinburgh, Reprinted 1958).

David, E., Z.Physik, 106, 206 (1937).

Dumin, D.J., Rev.Sci.Instrum., 38, 1107-9 (1967).

Fewkes, J.H., and Yarwood, J., Electricity and Magnetism, Vol.1, (University Tutorial Press, Cambridge, 1965).

Fochs, P.D., J.Opt.Soc.Amer., 40, 690 (1950).

Freiser, M.J., I.E.E.E. Trans. on Magnetics, Mag 4, 152-61, (1968).

Gillham, E.J., Nature, 178, 1412-3 (1956).

Hayfield, P.C.S., and White, G.W.T., Ellipsometry in the Measurement of Surfaces and Thin Films, 157-99, (E. Passaglia, R.R. Stromberg, and J. Kruger, Eds., Natl. Bur. Std. Misc. Publ. 256, U.S. Govt. Printing Office, Washington, 1964).

Heavens, O.S., Reports on Progress in Physics, 23, 1-65 (1960).

Heavens, O.S., /

Heavens, O.S., Optical Properties in Thin Solid Films (Dover Publications, Inc., New York, 1965).

Heavens, O.S., and Smith, S.D., J.Opt.Soc.Amer., 47 469-72 (1957).

Holmes, D.A., and Feucht, D.L., J.Opt.Soc.Amer., 57, 466 (1967).

Jacquinot, P., Rev.Opt. 21, 15 (1942).

King, R.J., and Downs, M.J., Surf.Sci. 16, 288-302 (1969).

King, R.J., and Talim, S.P., J.Phy.E: Sci.Instrum., 4 93-6 (1971).

McCrackin, F.L., Passaglia, E., Stromberg, R.R., and Steinberg, H.L., J.Res.Natl.Bur.Std.A., 67A, 363-77 (1963).

MacLeod, H.A., Thin Film Optical Filters, 27-9 (Adam Hilger Ltd., London, 1969).

Malé, D., Thèse, Université de Paris (1952).

Mayer, H., Physik dünner Schichten, 1 (Wissenschaftluhe Verlag, Stuttgart, 1950).

Muller, R.H., Surf.Sci., 16, 14-33 (1969).

Murmann, H., Z.Physik, 80, 161 (1933).

Neal, W.E.J., and Fane, R.W., J.Phy.E: Sci.Instrum., 6, 409-16 (1973).

Passaglia, E., (Ed.)., Ellipsometry in the Measurement of Surfaces and Thin Films (Natl.Bur.Std.Misc., Publ. 256, U.S. Govt. Printing Office, Washington, 1964).

Pliskin, W.A., and Conrad, E.E., I.B.M. J.Rev.Devolop, 8, 43 (1964).

Rothen A., Rev .Sci.Instrum., 16, 26-30 (1945).

Rouard, P., and Bousquet, P., Progress in Optics, Vol.4, 145-97, (North-Holland Publishing Co., Amsterdam, 1965).

Schopper, H., Ibid., 131, 215 (1952).

Schultz, L.G., J.Opt.Soc.Amer., 40, 623 (1950).

Shurcliff, W.A., /

Shurcliff, W.A., Polarized Light, Production and Use, (Oxford University Press, Oxford 1962).

Smith, P.H., Surf.Sci., 16, 34-66 (1969).

Surface Science, Vol. 16, (North-Holland Publishing Co., Amsterdam, 1969).

Takasaki, H., J.Opt.Soc.Amer., 51, 463 (1961).

Tenquist, D.W., Whittle, R.M., and Yarwood, J., University Optics, Vol.2, 1-33, (London Iliffe Books, 1970).

Tolansky, S., Surface Microtopography, (John Wiley and Sons, Inc., New York, 1960).

Vašíček, A. J.Opt.Soc.Amer., 37, 145-53 (1947).

Vašíček, A. J.Opt.Soc.Amer., 37, 979-80 (December, 1947).

Vašíček, A. Optics of Thin Films, 9-159, (North-Holland Publishing Co., Amsterdam, 1960).

Welsky, V.G., The Theory and Design of Inductance Coils, 40-68, (Macdonald, London, 1960).

Williamson, S.J., Weingart, J.M., and Andrews, R.D., J.Opt.Soc. Amer., 54, 337-41 (1964).

Winterbottom, A.B., Ellipsometry in the Measurement of Surfaces and Thin Films, 97-111, (E.Passaglia, R.R. Stromberg, and J. Kruger, Eds., Natl.Bur.Std.Misc.Publ. 256, U.S. Govt. Printing Office, Washington, 1964).

Wolter, H., Z.Physik, 105, 269 (1937).

APPENDIX I - The Computer Program

```
      ELLIPSOMETRY RESEARCH PROGRAM                                          1
      DIMENSION A0(50),A1(50),A2(50),FN0(50),FN1(50),FN2(50),PHI0(50),D12
     1(50),CHI(50),GAMMA(50),DELTA(50),PSI(50),ATLED(50),YSP(50),QHU(50,
     22),FN1A(50),WL(50),P(50),S(50)
      COMPLEX R,CFN2,Z,Z1,CK,ROOT1,ROOT2,RK1,RK2,RK3                         4
      PI=4.0*ATAN(1)                                                         5
      READ(7,10)M,N,IRUN,IDAY,MONTH,IYEAR
   10 FORMAT(6I0)
      WRITE(2,11)IRUN,IDAY,MONTH,IYEAR
   11 FORMAT(37H0ELLIPSOMETRY RESEARCH PROGRAM RUN NO,I5,2I3,I5)
      DO 20 J=1,N                                                            8
   20 READ(7,21)A0(J),A1(J),A2(J),FN0(J),FN1(J),PHI0(J),D1(J)                9
   21 FORMAT(7F0.0)                                                         10
      WRITE(2,22)                                                           11
   22 FORMAT(21H0CHECK OF INPUT DATA )
      DO 30 J=1,N                                                           13
   30 WRITE(2,31)A0(J),A1(J),A2(J),FN0(J),FN1(J),PHI0(J),D1(J)              14
   31 FORMAT(7(F8.2,2X))                                                    15
      WRITE(2,32)                                                           16
   32 FORMAT(62H0 DELTA(DEG)  PSI(DEG)  D1(ANGS)  REFRACTIVE INDEX  PHI017
     2(DEG) )                                                               18
      DO 40 J=1,N                                                           19
      CHI(J)=(A1(J)-A0(J))*(PI/180)+(PI/2)                                  20
      GAMMA(J)=(A2(J)-A1(J))*(PI/180)                                       21
      B=2.0*CHI(J)                                                          22
      ALFA=SIN(B)/COS(B)                                                    23
      C=2.0*GAMMA(J)                                                        24
      BETA=SIN(C)                                                           25
      D=SQRT((ALFA*ALFA+BETA*BETA)/(1-BETA*BETA))                           26
      PSI(J)=0.5*ATAN(D)                                                    27
      E=SIN(C)/COS(C)                                                       28
      DELTA(J)=ATAN2(E,SIN(B))                                              29
      QHU(J,1)=(SIN(PSI(J))/COS(PSI(J)))*COS(DELTA(J))
      QHU(J,2)=(SIN(PSI(J))/COS(PSI(J)))*SIN(DELTA(J))
      ATLED(J)=DELTA(J)*(180/PI)                                            32
      YSP(J)=PSI(J)*(180/PI)                                                33
      WRITE(2,33)ATLED(J),YSP(J),D1(J),FN1(J),PHI0(J)                       34
   33 FORMAT(F12.5,F10.4,F11.3,F14.4,F14.5)                                 35
   40 CONTINUE                                                              36
      GOTO(900,50,70,130),M                                                 37
   50 WRITE(2,51)                                                           38
   51 FORMAT(97H0REFRACTIVE INDEX OF BARE SUBSTRATE  ABSORBTION COEFF OF
     3 BARE SUBSTRATE  PHI0(DEG)  ERROR IN N2  )
      DO 60 J=1,N                                                           41
      R=CMPLX(QHU(J,1),QHU(J,2))
      PH=PHI0(J)*(PI/180)                                                   43
      Z=1-(4*R*SIN(PH)*SIN(PH))/((R+1)*(R+1))                               44
      CFN2=FN0(J)*(SIN(PH)/COS(PH))*CSQRT(Z)                                45
      ERCFN2=(CABS(CFN2)-REAL(CFN2))
      WRITE(2,52)CFN2,PHI0(J),ERCFN2
   52 FORMAT(10X,F12.6,27X,F11.6,13X,F8.3,3X,F11.7)
```

```
 60 CONTINUE                                                          49
    GOTO 900                                                          50
 70 DO 80 J=1,N                                                       51
 80 READ(7,81)FN2(J),WL(J)
 81 FORMAT(2F0.0)                                                     53
    WRITE(2,82)                                                       54
 82 FORMAT(63HOKNOWN REFRACT IND OF FILM  THICKNESS OF FILM(ANG)  ERRO
   4R(ANG) )
    DO 120 J=1,N                                                      57
    PHO=PHIO(J)*(PI/180)                                              58
    CSP1=SQRT(1-(FNO(J)*SIN(PHO)/FN1(J))**2)                          59
    RP01=(FN1(J)*COS(PHO)-FNO(J)*CSP1)/(FN1(J)*COS(PHO)+FNO(J)*CSP1)  60
    RS01=(FNO(J)*COS(PHO)-FN1(J)*CSP1)/(FNO(J)*COS(PHO)+FN1(J)*CSP1)  61
    SSP1=SQRT(1-CSP1*CSP1)                                            62
    CSP2=SQRT(1-(FN1(J)*SSP1/FN2(J))**2)                              63
    RP12=(FN2(J)*CSP1-FN1(J)*CSP2)/(FN2(J)*CSP1+FN1(J)*CSP2)          64
    RS12=(FN1(J)*CSP1-FN2(J)*CSP2)/(FN1(J)*CSP1+FN2(J)*CSP2)          65
    Z1=CMPLX(0.0,DELTA(J))                                            66
    CK=CEXP(Z1)*(SIN(PSI(J))/COS(PSI(J)))                             67
    P1RK1=RS12*RP01*RP12                                              68
    P2RK1=RP12*RS01*RS12                                              69
    P1RK2=RS01*RP01*RP12+RS12                                         70
    P2RK2=RP12*RP01*RS01*RS12                                         71
    RK1=CK*P1RK1-P2RK1                                                72
    RK2=CK*P1RK2-P2RK2                                                73
    RK3=CK*RS01-RP01                                                  74
    ROOT1=(-RK2+CSQRT(RK2*RK2-4.0*RK1*RK3))/(2.0*RK1)                 75
    ROOT2=(-RK2-CSQRT(RK2*RK2-4.0*RK1*RK3))/(2.0*RK1)                 76
    DAR=ALOG(CABS(ROOT1))                                             77
    RROOT1=REAL(ROOT1)                                                78
    AROOT1=AIMAG(ROOT1)                                               79
    DAI=ATAN2(-AROOT1,RROOT1)                                         80
    DBR=ALOG(CABS(ROOT2))                                             81
    RROOT2=REAL(ROOT2)                                                82
    AROOT2=AIMAG(ROOT2)                                               83
    DBI=ATAN2(-AROOT2,RROOT2)                                         84
    DRA=(DAR*WL(J))/(FN1(J)*CSP1*4.0*PI)
    DRB=(DBR*WL(J))/(FN1(J)*CSP1*4.0*PI)
    DIFF=ABS(DAR)-ABS(DBR)                                            85
    IF(DIFF)90,90,100                                                 86
 90 DR=(DAI*WL(J))/(FN1(J)*CSP1*4.0*PI)
    ERDR=SQRT(DRA*DRA+DR*DR)-DR
    GOTO 110                                                          89
100 DR=(DBI*WL(J))/(FN1(J)*CSP1*4.0*PI)
    ERDR=SQRT(DRB*DRB+DR*DR)-DR
110 WRITE(2,111)FN1(J),DR,ERDR                                        92
111 FORMAT(8X,F12.6,12X,F12.4,7X,F7.4)                                93
120 CONTINUE                                                          94
    GOTO 900                                                          95
130 WRITE(2,132)
132 FORMAT(66HO PSI(DEG)  DELTA(DEG)  REFRACT IND  THICKNESS(ANG)  ER
   5ROR(ANG)  )
    DO 133 J=1,N
133 READ(7,134)FN2(J),WL(J),P(J),S(J)
134 FORMAT(4F0.0)
    DO 170 J=1,N
    WRITE(2,135)YSP(J),ATLED(J)
135 FORMAT(F10.5,1X,F10.5)
    DO 170 K=1,20                                                     116
    FN1A(K)=P(J)
```

```
      PH0=PHI0(J)*(PI/180)
      CSP1=SQRT(1-(FN0(J)*SIN(PH0)/FN1A(K))*(FN0(J)*SIN(PH0)/FN1A(K)))
      RP01=(FN1A(K)*COS(PH0)-FN0(J)*CSP1)/(FN1A(K)*COS(PH0)+FN0(J)*CSP1)
      RS01=(FN0(J)*COS(PH0)-FN1A(K)*CSP1)/(FN0(J)*COS(PH0)+FN1A(K)*CSP1)
      SSP1=SQRT(1-CSP1*CSP1)                                          122
      CSP2=SQRT(1-(FN1A(K)*SSP1/FN2(J))*(FN1A(K)*SSP1/FN2(J)))
      RP12=(FN2(J)*CSP1-FN1A(K)*CSP2)/(FN2(J)*CSP1+FN1A(K)*CSP2)
      RS12=(FN1A(K)*CSP1-FN2(J)*CSP2)/(FN1A(K)*CSP1+FN2(J)*CSP2)
      Z1=CMPLX(0.0,DELTA(J))                                          126
      CK=CEXP(Z1)*(SIN(PSI(J))/COS(PSI(J)))                           127
      P1RK1=RS12*RP01*RP12                                            128
      P2RK1=RP12*RS01*RS12                                            129
      P1RK2=RS01*RP01*RP12+RS12                                       130
      P2RK2=RP12+RP01*RS01*RS12                                       131
      RK1=CK*P1RK1-P2RK1                                              132
      RK2=CK*P1RK2-P2RK2                                              133
      RK3=CK*RS01-RP01                                                134
      ROOT1=(-RK2+CSQRT(RK2*RK2-4.0*RK1*RK3))/(2.0*RK1)               135
      ROOT2=(-RK2-CSQRT(RK2*RK2-4.0*RK1*RK3))/(2.0*RK1)               136
      DARA=ALOG(CABS(ROOT1))                                          137
      RROOT1=REAL(ROOT1)                                              138
      AROOT1=AIMAG(ROOT1)                                             139
      DAIA=ATAN2(-AROOT1,RROOT1)
      DBRA=ALOG(CABS(ROOT2))                                          141
      RROOT2=REAL(ROOT2)                                              142
      AROOT2=AIMAG(ROOT2)                                             143
      DBIA=ATAN2(-AROOT2,RROOT2)
      DRAA=(DARA*WL(J))/(FN1A(K)*CSP1*4.0*PI)
      DRBA=(DBRA*WL(J))/(FN1A(K)*CSP1*4.0*PI)
      DIFF=ABS(DARA)-ABS(DBRA)                                        145
      IF(DIFF)140,140,150                                             146
  140 DRA=(DAIA*WL(J))/(FN1A(K)*CSP1*4.0*PI)
      ERDRA=SQRT(DRAA*DRAA+DRA*DRA)-DRA
      GOTO 160                                                        149
  150 DRA=(DBIA*WL(J))/(FN1A(K)*CSP1*4.0*PI)
      ERDRA=SQRT(DRBA*DRBA+DRA*DRA)-DRA
  160 WRITE(2,161)FN1A(K),DRA,ERDRA
  161 FORMAT(24X,F11.5,2X,F12.4,4X,F7.3)
      P(J)=P(J)+S(J)
  170 CONTINUE                                                        155
  900 STOP
      END
```

APPENDIX II

KEY TO THE COMPUTER PROGRAM

Subscripted VAriables

AO, Al, A2	The three analyzer readings A_0, A_1 and A_2
FNO, FNl, FN2	The refractive indices n_0, n_1 and n_2
PHIO	The angle of incidence ϕ_0
Dl	The known film thickness
CHI, GAMMA, DELTA, PSI	The angles χ, γ, Δ and ψ
QHU	The complex value of Q
FNIA, P, S	Assumed values of n_1 and the increment(S)

Complex Variables

R	Temporary storage for complex Q
CFN2	Complex computed refractive index of bare substrate
Z	Temporary store
Zl	Temporary storage for $i\Delta$
CK	Temporary storage for $\exp(i\Delta)\tan\psi$
ROOTl, ROOT2	Roots of quadratic in exp(-D)
RKl, RK2, RK3	Factors k_1, k_2 and k_3 in quadratic

Non-Dimensionable Variables

M	Calculation control
N	Number of sets of results
B, C, D, E	Temporary stores
PH, PHO	Value of ϕ_0 in radians
CSPN, SSPN	Cosine of ϕ_n, sign of ϕ_n (n=1,2)
RPOl, RSOl, RPl2, RSl2	Amplitude reflection coefficients
PlRKl	Part one of k_1
P2RKl /	

P2RK1	Part two of k_1
P1RK2	Part one of k_2
P2RK2	Part two of k_2
DAR, DAI, DBR, DBI	Phase thickness D for real and imaginary parts of roots q and v
DARA, DAIA, DBRA, DBIA	Phase thickness D for assumed values of refractive index n_1
DR, DRA	Computed film thickness d_1
ERDR, ERDRA	Error in d_1

Functions

ATAN2(X,Y)	Arctan(X/Y) in (O, 2π)
SQRT(X)	Square root of x
CMPLX(X)	Express real arguments of x in complex form
CABS(X)	Modulus of complex x
REAL(X)	Real part of complex x
IMAG(X)	Imaginary part of complex x
CEXP(X)	Complex exponent of x
ALOG(X)	Natural logarithm of x
SIN(X), COS(X)	Sine and cosine of x

APPENDIX III - The Reflectance Spectrophotometer Scans of the MgF_2 Films

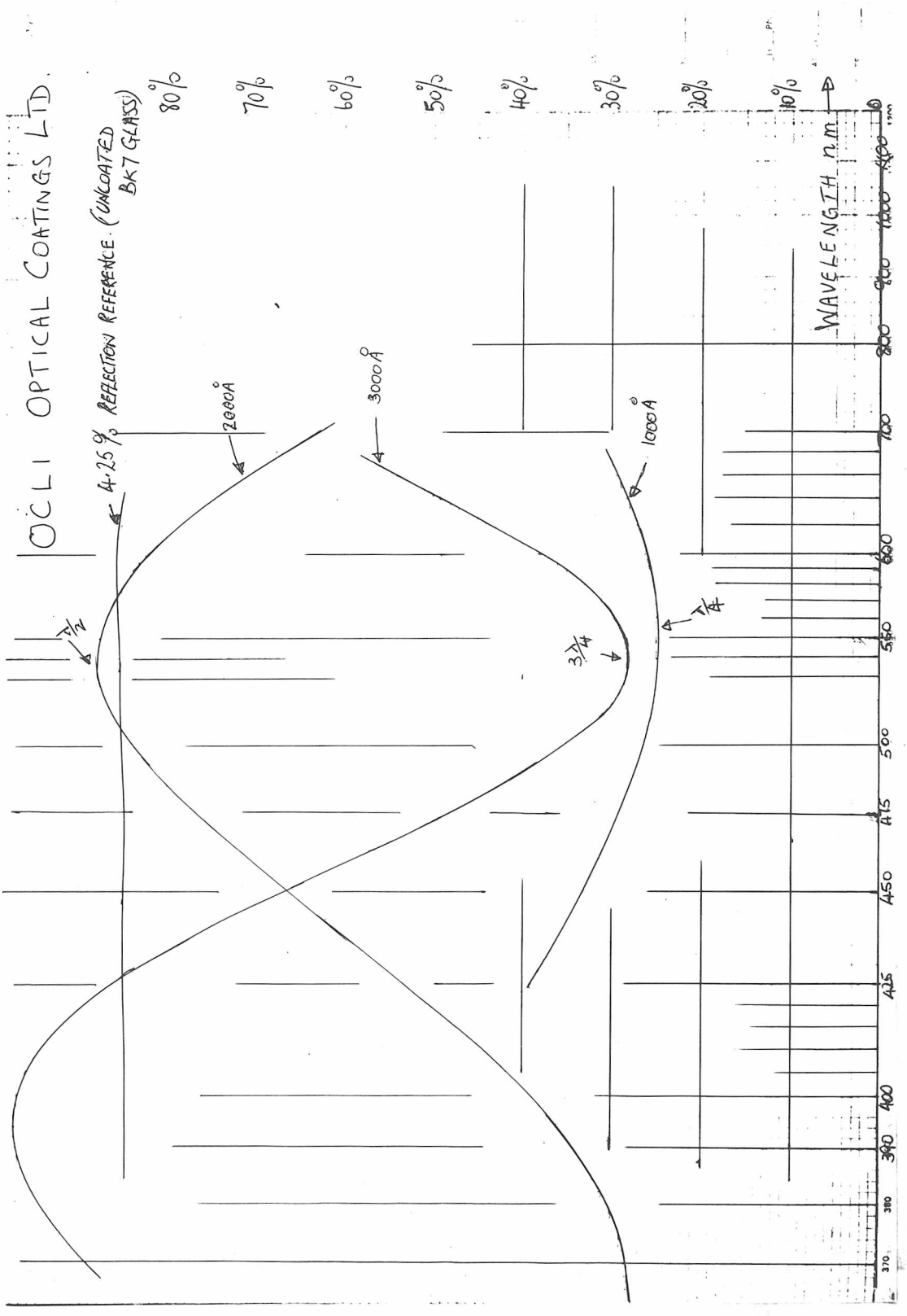

OCLI OPTICAL COATINGS Ltd.

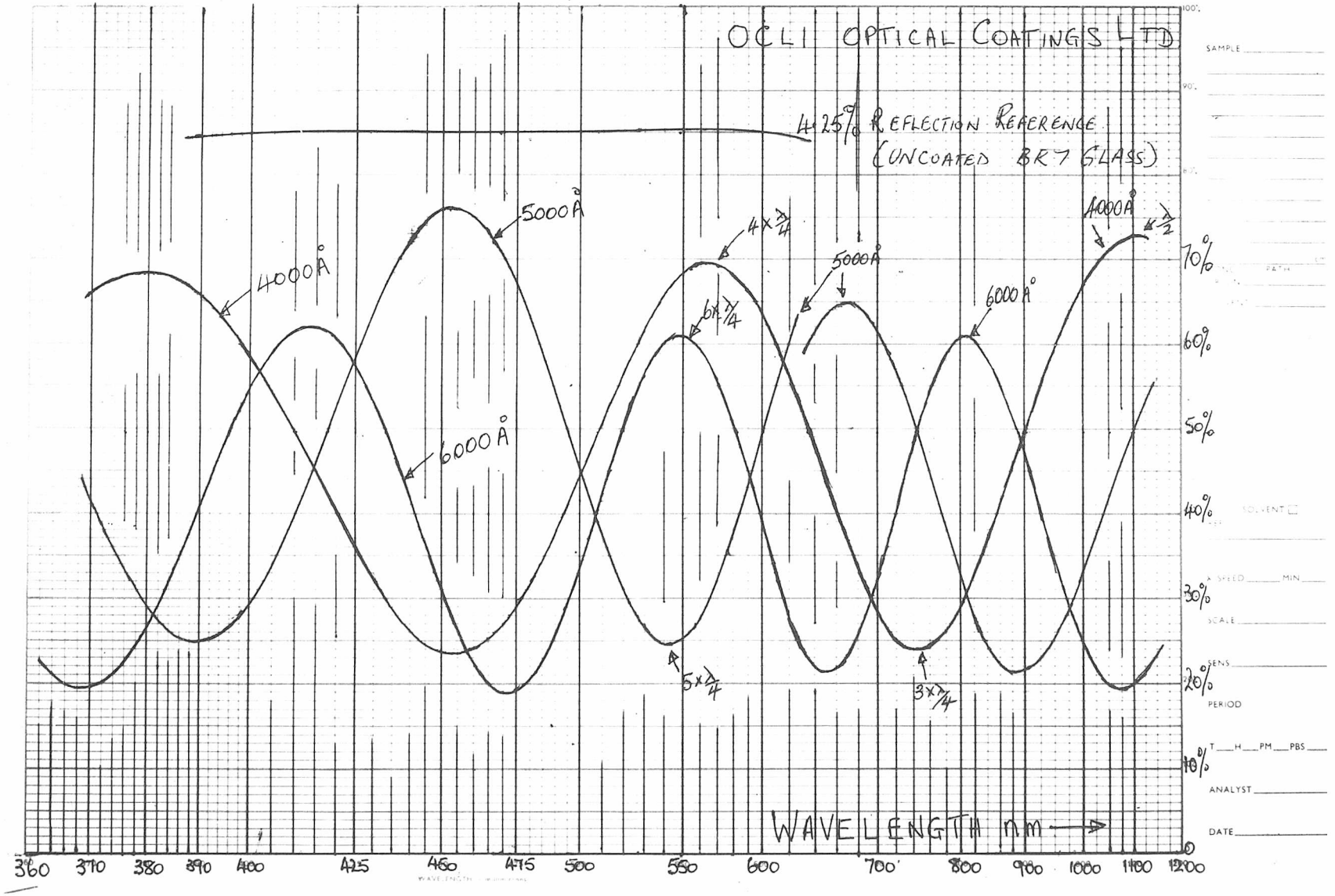

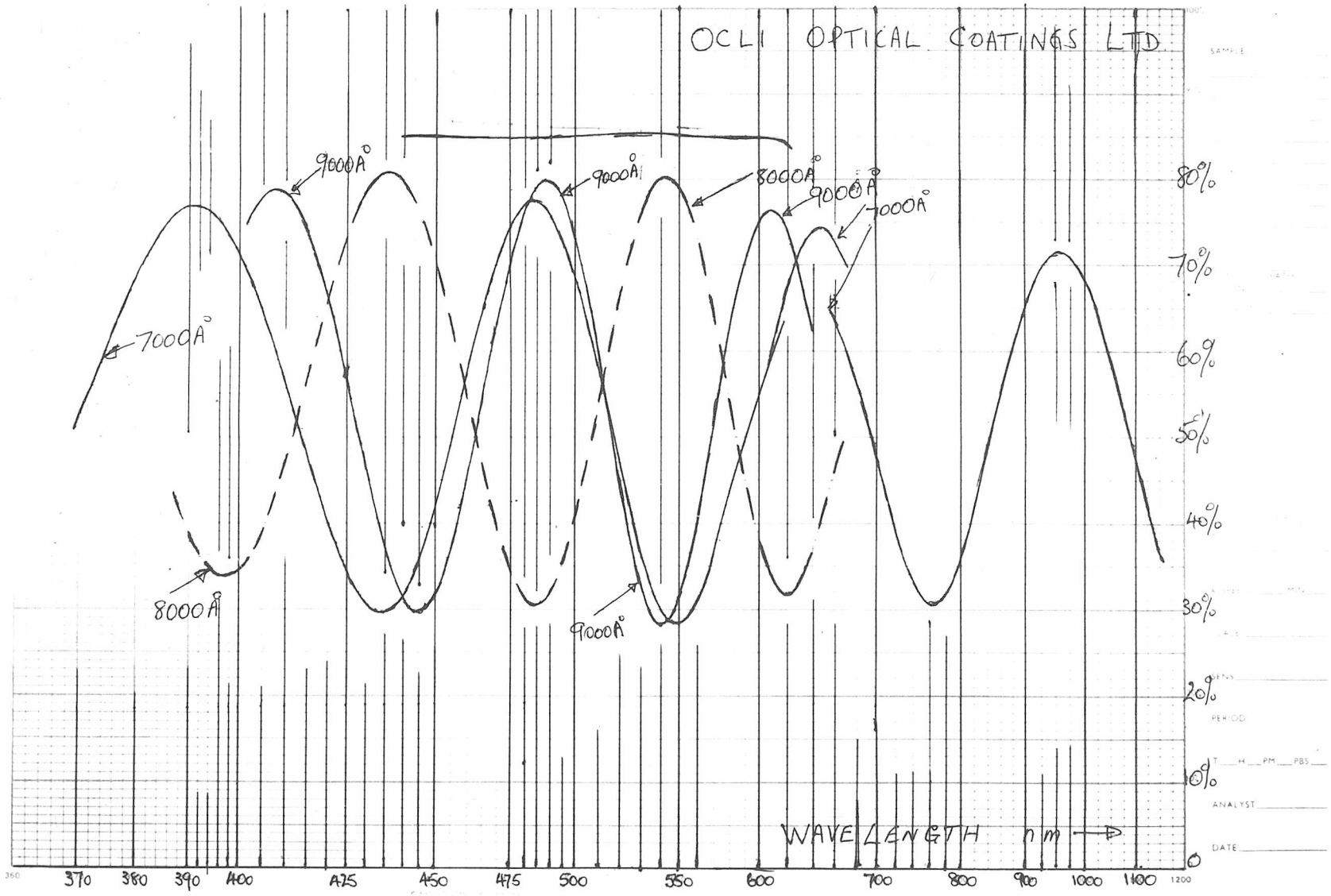
OCLI OPTICAL COATINGS LTD.
9000Å
9000Å
8000Å
9000Å
7000Å
7000Å
8000Å
9000Å
80%
70%
60%
50%
40%
30%
20%
10%
0
WAVELENGTH nm
360
370
380
390
400
425
450
475
500
550
600
700
800
900
1000
1100
1200

APPENDIX IV - List of Component Suppliers

1.	Source	G.E.C. Tungsten Halogen Projector Lamp A1/216 24V 150W - Local Supplier
2.	Lamp supply	Linstead Power Supply Type S4A - Linstead Electronics Roslyn Works, Roslyn Rd, London, N15 5JB
3.	Monochromatic filter	5461Å Narrow Band Filter - Barr & Stroud Ltd., Caxton St., Anniesland, Glasgow, G13 1HZ
4.	Vertical divided circles	Precision Tools Instruments Ltd. (P.T.I.), Calibrated Divided Circles - Ealing Beck Ltd., 15 Greycaine Rd., Watford, WD2 4PW
5.	λ/-plate (unmounted) for 5461Å wavelength	- F. Wiggins & Sons Ltd., 9 Tredown Rd., Sydenham, SE26
6.	Collimator, telescope and turntable	P.T.I. Advanced Spectrometer - Griffin & George Ltd., 285 Ealing Road, Wembley, HAO 1HJ
7.	Polarizers	Ks-MIK polarizing filters - E. Käsemann, Optische Werkstatten GmbH, 8203 Oberaudorf, W. Germany

8.	Faraday cell core	Schott SF57 NSFK quality optical glass - H.V. Skan Ltd, 425-433 Stratford Road, Shirley, Solihull, Warwickshire, B90 4AE
9.	Photomultiplier	RCA 931A - RCA Ltd., Sunbury-on-Thames, Middlesex, TW16 7HW
10.	Magnetic shielding	Telshield - Telcon Metals Ltd., Manor Royal, Crawley, Sussex
11.	E.H.T. Supply	Wallis 2.5kV, 4mA Type 2PM - Wallis Electronics Ltd., Worthing, Sussex
12.	Oscilloscope	Telequipment D83 - Telequipment Ltd., 313 Chase Rd., Southgate, London, N14 6JJ
13.	Optical benches and saddles	- Ealing Beck Ltd., 15 Greycaine Rd., Watford, WD2 4PW